



HAL
open science

Projected land ice contributions to twenty-first-century sea level rise

Tamsin L. Edwards, Sophie M.J. Nowicki, Ben Marzeion, Regine Hock, Heiko Goelzer, H el ene Seroussi, Nicolas Jourdain, Donald A. Slater, Fiona E. Turner, Christopher J. Smith, et al.

► To cite this version:

Tamsin L. Edwards, Sophie M.J. Nowicki, Ben Marzeion, Regine Hock, Heiko Goelzer, et al.. Projected land ice contributions to twenty-first-century sea level rise. *Nature*, 2021, 593 (7857), pp.74-82. 10.1038/s41586-021-03302-y . hal-03230877

HAL Id: hal-03230877

<https://hal.science/hal-03230877>

Submitted on 16 Sep 2021

HAL is a multi-disciplinary open access archive for the deposit and dissemination of scientific research documents, whether they are published or not. The documents may come from teaching and research institutions in France or abroad, or from public or private research centers.

L'archive ouverte pluridisciplinaire **HAL**, est destin ee au d ep ot et  a la diffusion de documents scientifiques de niveau recherche, publi es ou non,  emanant des  tablissements d'enseignement et de recherche fran ais ou  trangers, des laboratoires publics ou priv es.

ARTICLE

Projected land ice contributions to 21st century sea level rise

Tamsin L. Edwards^{1*}, Sophie Nowicki^{2,58}, Ben Marzeion^{6,7}, Regine Hock^{14,52}, Heiko Goelzer^{3,4,53}, H el ene Seroussi⁵, Nicolas C. Jourdain⁹, Donald Slater^{10,51}, Fiona Turner¹, Christopher J. Smith⁸, Christine M. McKenna⁸, Erika Simon², Ayako Abe-Ouchi¹¹, Jonathan M. Gregory^{12,13}, Eric Larour⁵, William H. Lipscomb¹⁵, Antony J. Payne¹⁶, Andrew Shepherd¹⁷, C ecile Agosta¹⁸, Patrick Alexander^{19,20}, Torsten Albrecht²¹, Brian Anderson²², Xylar Asay-Davis²³, Andy Aschwanden¹⁴, Alice Barthel²³, Andrew Bliss²⁴, Reinhard Calov²¹, Christopher Chambers²⁵, Nicolas Champollion^{6,9}, Youngmin Choi^{26,5}, Richard Cullather², Joshua Cuzzone⁵, Christophe Dumas¹⁸, Denis Felikson^{2,57}, Xavier Fettweis²⁸, Koji Fujita²⁹, Benjamin K. Galton-Fenzi^{27,44}, Rupert Gladstone⁴⁷, Nicholas R. Golledge²², Ralf Greve^{25,56}, Tore Hattermann^{30,31}, Matthew J. Hoffman²³, Angelika Humbert^{32,48}, Matthias Huss^{33,34,35}, Philippe Huybrechts³⁶, Walter Immerzeel³⁷, Thomas Kleiner³², Philip Kraaijenbrink³⁷, S ebastien Le clec'h³⁶, Victoria Lee³⁸, Gunter R. Leguy¹⁵, Christopher M. Little³⁹, Daniel P. Lowry⁴⁹, Jan-Hendrik Malle^{6,7}, Daniel F. Martin⁵⁰, Fabien Maussion⁴⁰, Mathieu Morlighem²⁶, James F. O'Neill¹, Isabel Nias^{2,55}, Frank Pattyn⁴, Tyler Pelle²⁶, Stephen Price²³, Aur elien Quiquet¹⁸, Valentina Radi c⁴¹, Ronja Reese²¹, David R. Rounce¹⁴, Martin R uckamp³², Akiko Sakai²⁹, Courtney Shafer⁵⁰, Nicole-Jeanne Schlegel⁵, Sarah Shannon¹⁶, Robin S. Smith¹², Fiammetta Straneo¹⁰, Sainan Sun⁴, Lev Tarasov⁴², Luke D. Trusel⁴³, Jonas Van Breedam³⁶, Roderik van de Wal^{3,37}, Michiel van den Broeke³, Ricarda Winkelmann^{21,54}, Harry Zekollari^{45,4,33,34}, Chen Zhao⁴⁴, Tong Zhang²³, Thomas Zwinger⁴⁶

* Corresponding author

1 Department of Geography, King's College London, London, UK

2 NASA Goddard Space Flight Center, Greenbelt, MD, USA

3 Institute for Marine and Atmospheric research Utrecht, Utrecht University, The Netherlands

4 Laboratoire de Glaciologie, Universit e Libre de Bruxelles, Brussels, Belgium

5 Jet Propulsion Laboratory, California Institute of Technology, Pasadena, CA, USA

32 6 Institute of Geography, University of Bremen, Germany
33 7 MARUM – Center for Marine Environmental Sciences, University of Bremen, Germany
34 8 Priestley International Centre for Climate, University of Leeds, Leeds, UK
35 9 Univ. Grenoble Alpes/CNRS/IRD/G-INP, Institut des Géosciences de l'Environnement, France
36 10 Scripps Institution of Oceanography, University of California San Diego, La Jolla, CA, USA
37 11 Atmosphere and Ocean Research Institute, The University of Tokyo, Kashiwa-shi, Chiba 277-8564,
38 Japan
39 12 National Centre for Atmospheric Science, University of Reading, Reading, UK
40 13 Met Office, Hadley Centre, Exeter, UK
41 14 Department of Civil and Environmental Engineering, Carnegie Mellon University, USA
42 15 Climate and Global Dynamics Laboratory, National Center for Atmospheric Research, Boulder, CO,
43 USA
44 16 School of Geographical Sciences, University of Bristol, Bristol, UK
45 17 Centre for Polar Observation and Modelling, School of Earth and Environment, University of Leeds,
46 Leeds, LS2 9JT, UK
47 18 Laboratoire des sciences du climat et de l'environnement, LSCE-IPSL, CEA-CNRS-UVSQ, Université
48 Paris-Saclay, France
49 19 Lamont-Doherty Earth Observatory, Columbia University, Palisades, NY, USA
50 20 NASA Goddard Institute for Space Studies, New York, NY, USA
51 21 Potsdam Institute for Climate Impact Research (PIK), Member of the Leibniz Association, Potsdam,
52 Germany
53 22 Antarctic Research Centre, Victoria University of Wellington, New Zealand
54 23 Theoretical Division, Los Alamos National Laboratory, Los Alamos, NM, USA
55 24 Department of Anthropology and Geography, Colorado State University, USA
56 25 Institute of Low Temperature Science, Hokkaido University, Sapporo, Japan
57 26 Department of Earth System Science, University of California Irvine, Irvine, CA, USA
58 27 Australian Antarctic Division, Kingston, Tasmania, Australia
59 28 Laboratory of Climatology, Department of Geography, University of Liège, Liège, Belgium
60 29 Graduate School of Environmental Studies, Nagoya University, Nagoya, Japan
61 30 Norwegian Polar Institute, Tromsø, Norway
62 31 Energy and Climate Group, Department of Physics and Technology, The Arctic University – University
63 of Tromsø, Tromsø, Norway
64 32 Alfred-Wegener-Institut Helmholtz-Zentrum für Polar- und Meeresforschung, Bremerhaven, Germany
65 33 Laboratory of Hydraulics, Hydrology and Glaciology (VAW), ETH Zurich, Switzerland
66 34 Swiss Federal Institute for Forest, Snow and Landscape Research (WSL), Birmensdorf, Switzerland
67 35 Department of Geosciences, University of Fribourg, Switzerland
68 36 Earth System Science and Departement Geografie, Vrije Universiteit Brussel, Brussels, Belgium
69 37 Department of Physical Geography, Utrecht University, The Netherlands

- 70 38 Centre for Polar Observation and Modelling, School of Geographical Sciences, University of Bristol,
71 Bristol, UK
- 72 39 Atmospheric and Environmental Research, Inc., Lexington, Massachusetts, USA
- 73 40 Department of Atmospheric and Cryospheric Sciences, University of Innsbruck, Austria
- 74 41 Department of Earth, Ocean and Atmospheric Sciences, University of British Columbia, Canada
- 75 42 Dept of Physics and Physical Oceanography, Memorial University of Newfoundland, Canada
- 76 43 Department of Geography, Pennsylvania State University, University Park, PA, USA
- 77 44 Australian Antarctic Program Partnership, Institute for Marine and Antarctic Studies, University of
78 Tasmania, Hobart, Tasmania
- 79 45 Department of Geoscience and Remote Sensing, Delft University of Technology, The Netherlands
- 80 46 CSC-IT Center for Science, Espoo, Finland
- 81 47 Arctic Centre, University of Lapland, Finland
- 82 48 Department of Geoscience, University of Bremen, Bremen, Germany
- 83 49 GNS Science, Lower Hutt, New Zealand
- 84 50 Computational Research Division, Lawrence Berkeley National Laboratory, Berkeley, CA, USA
- 85 51 School of Geography and Sustainable Development, University of St Andrews, UK
- 86 52 Department of Geosciences, University of Oslo, Norway
- 87 53 NORCE Norwegian Research Centre, Bjerknes Centre for Climate Research, Bergen, Norway
- 88 54 Department of Physics and Astronomy, University of Potsdam, Potsdam, Germany
- 89 55 School of Environmental Sciences, University of Liverpool, Liverpool, UK
- 90 56 Arctic Research Center, Hokkaido University, Sapporo, Japan
- 91 57 Universities Space Research Association, Goddard Earth Sciences Technology and Research Studies
92 and Investigations, Columbia, MD 21044, USA
- 93 58 Geology Department and RENEW Institute, University at Buffalo, Buffalo, NY, USA

94

95 **The land ice contribution to global mean sea level rise has not yet been predicted¹ with**
96 **ice sheet and glacier models for the latest set of socio-economic scenarios, nor with**
97 **coordinated exploration of uncertainties arising from the various computer models**
98 **involved. Two recent international projects generated a large suite of projections using**
99 **multiple models^{2-3,5,8,14-16}, but mostly used previous generation scenarios⁹ and climate**
100 **models²¹, and could not fully explore known uncertainties. Here we estimate probability**
101 **distributions for these projections under the new scenarios^{19,30} using statistical**
102 **emulation of the ice sheet and glacier models, and find that limiting global warming to**
103 **1.5°C would halve the land ice contribution to 21st century sea level rise, relative to**
104 **current emissions pledges. The median decreases from 25 to 13 cm sea level equivalent**
105 **(SLE) by 2100, with glaciers responsible for half the sea level contribution. The**
106 **Antarctic contribution does not show a clear response to emissions scenario, due to**

107 **competing processes of increasing ice loss and snowfall accumulation in a warming**
108 **climate. However, under risk-averse (pessimistic) assumptions, Antarctic ice loss could**
109 **be five times higher, increasing the median land ice contribution to 42 cm SLE under**
110 **current policies and pledges, with the upper end (95th percentile) exceeding half a metre**
111 **even under 1.5°C warming. This would severely limit the possibility of mitigating future**
112 **coastal flooding. Given this large range (13 cm main projections under 1.5°C warming;**
113 **42 cm risk-averse projections under current pledges), adaptation must plan for a factor**
114 **of three uncertainty in the land ice contribution to 21st century sea level rise until**
115 **climate policies and the Antarctic response are further constrained.**

116

117 Land ice has contributed around half of all sea level rise since 1993, and this fraction is
118 expected to increase¹. The Ice Sheet Model Intercomparison Project (ISMIP6^{2,3}) for CMIP6⁴
119 and the Glacier Model Intercomparison Project (GlacierMIP⁵) provide the Intergovernmental
120 Panel on Climate Change (IPCC) with projections of Earth's ice sheet and glacier
121 contributions to future sea level. Both projects use suites of numerical models^{6,7,8} and
122 greenhouse gas emission scenarios⁹ as the basis of their projections, and a variety of
123 treatments are considered for the interaction between the ice sheets and the ocean^{10,11,12,13}. In
124 total, the projects provide 256 simulations of the Greenland ice sheet, 344 simulations of the
125 Antarctic ice sheet, and 288 simulations of the global glacier response to climate change
126 ^{8,14,15,16} (see also Extended Data Table 1). Although these simulations represent an
127 unprecedented effort ^{3,6,7,8,10-18}, their computational expense and complexity has meant that
128 they (i) focus mainly on previous generation emissions scenarios (Representation
129 Concentration Pathways⁹, RCPs) developed for the IPCC's Fifth Assessment Report, not the
130 more diverse and policy-relevant Shared Socioeconomic Pathways (SSPs^{19,20}) that underpin
131 the IPCC's Sixth Assessment Report, (ii) are driven mostly by a relatively small number of
132 older generation global climate models developed before CMIP6²¹, and (iii) have incomplete
133 and limited ensemble designs.

134

135 To address these limitations, we emulate the future sea level contribution of the 23 regions
136 comprising the world's land ice (see Extended Data Table 2) as a function of global mean
137 surface air temperature change and as a consequence of marine-terminating glacier retreat in
138 Greenland and ice-shelf basal melting and collapse in Antarctica. The ensembles of ice sheet
139 and glacier models are emulated all at once for each region, using their simulations as

140 multiple estimates of sea level contribution for a given set of uncertain input values, and we
141 incorporate the ensemble spread through the use of a ‘nugget’ term in Gaussian Process
142 emulation^{22,23}. Gaussian Process regression requires minimal assumptions about the
143 functional form, and provides uncertainty estimates for the emulator predictions²⁴; most
144 previous emulator-type approaches for sea level rise use parametric models, where the
145 functional form is assumed²⁵⁻²⁹. We then use the emulators to make probabilistic projections
146 for the glacier and ice sheet sea level contributions under five SSPs and under an additional
147 scenario reflecting current climate pledges (Nationally Determined Contributions, NDCs)³⁰
148 made under the Paris Agreement. Most projections presented are for the year 2100, but we
149 also estimate a full timeseries by emulating each year from 2016 to 2100. The details of our
150 emulation approach are described in the Methods.

151

152 **Response to temperature and parameters**

153

154 Most land ice regions show a fairly linear relationship of increasing mass loss with global
155 mean surface air temperature. Figure 1 shows the temperature-dependence of the sea level
156 contribution at 2100 for the ice sheets and peripheral glaciers (Fig. 1 a-f) and eleven other
157 glacier regions: four with large maximum contributions (Alaska, Arctic Canada North and
158 South, Russian Arctic: Fig. 1g-j), two with non-linear temperature-dependence, giving near
159 or total disappearance at high temperatures (Central Europe and Caucasus: Fig. 1k, l), and the
160 three regions comprising High Mountain Asia (Fig. 1m-o), which are important for local
161 water supply³². Values of ice sheet parameters are fixed at two possible values for Greenland
162 glacier retreat and Antarctic basal melting, with no Antarctic ice shelf collapse; only
163 simulations using these values are shown. The ensemble designs are not complete – for
164 example, many fewer ice sheet simulations were performed under RCP2.6 than RCP8.5 – so
165 some of the apparent patterns in the simulation data are artefacts of the gaps, which the
166 emulator is intended to account for.

167

168 Greenland and the glaciers, which are dominated by surface melting^{8,14,16}, show clear
169 dependence on temperature. Fourteen of the nineteen glacier regions show approximately
170 linear relationships, and five are nonlinear (Fig. 1f, k, l; also Western Canada & U.S. and
171 North Asia, which have weaker nonlinearity: not shown). In contrast, East Antarctica (Fig.
172 1c) shows a slight decrease in sea level contribution with temperature: snowfall increases,

173 because warmer air can hold more water vapour, and this dominates over the increase in mass
174 loss due to melting^{15,16}. Finally, West Antarctica and the Peninsula (b, e) show little
175 detectable temperature-dependence, due to an approximate cancellation across varying
176 climate and ice sheet model predictions of snowfall accumulation and ice loss. Antarctic ice
177 sheet results are discussed in detail later (see 'Antarctic focus').

178

179 The ice sheet contributions depend strongly on the Greenland glacier retreat and Antarctic
180 sub-shelf basal melting parameters, which determine the sensitivity of the marine-terminating
181 glaciers to ocean temperatures (and surface meltwater runoff for Greenland). Figure 2 shows
182 these relationships; the Greenland parameter is defined such that more negative values
183 correspond to further retreat inland.

184

185 **Land ice contributions in 2100**

186

187 We use probability distributions for global mean surface air temperature (Fig. 3a: FaIR
188 simple climate model³⁰) and ice-ocean parameters (Figs. 3b and 3c show κ and γ , which are
189 derived from the original parameterisation studies; ice shelf collapse is assigned equal
190 probability off/on) as inputs to the emulators. Time series projections for the land ice
191 contribution under all scenarios are shown in Fig. 3d, and probability density functions at
192 2100 for the Greenland ice sheet, Arctic Canada North, the glacier total, and West and East
193 Antarctica in Fig. 3e-i. The Antarctic ice sheet total under the NDCs is shown in (j). ('Risk-
194 averse' projections in (d) and (j) are discussed later.) Density estimates are less smooth for the
195 glacier and Antarctica totals than individual regions, because sums of regions are estimated
196 by random sampling rather than deterministic integration; these samples are shown for
197 Antarctica (j).

198

199 Our projections show that reducing greenhouse gas emissions from current and projected
200 pledges under the Paris Agreement (NDCs) enough to limit warming to 1.5 °C (SSP1-19)
201 would nearly halve the land ice contribution to sea level at 2100 (Table 1: median decreases
202 from 25 cm to 14 cm SLE). This halving is not evenly distributed across the three ice
203 sources: Greenland ice sheet mass losses would reduce by 70%, glacier mass losses by about
204 half, and Antarctica shows no significant difference between scenarios; this is not due to a

205 lack of change in the Antarctica simulations themselves, but rather to the cancellation of mass
206 gains and losses mentioned above.

207

208 Average rates of mass loss for each ice sheet and the glacier total are within 1-2 cm/century,
209 of those of the 2013 IPCC Fifth Assessment Report²⁵ (see Methods: Comparison with IPCC
210 assessments), and the updated assessment for RCP2.6 in the 2019 IPCC Special Report on
211 the Oceans and Cryosphere in a Changing Climate (SROCC)¹. However, SROCC revised the
212 projection for Antarctica under RCP8.5 up to 11 cm/century, close to the upper end of our
213 66% interval for SSP5-85 (though our projections may omit a commitment contribution of up
214 to about 2 cm/century; see Methods). Our results are therefore closer to the 2013 than 2019
215 IPCC assessment regarding the magnitude and unclear scenario-dependence for Antarctica.
216 Our 66% uncertainty intervals are narrower than the IPCC 66% (SROCC) and $\geq 66\%$ (AR5)
217 uncertainty intervals, as would be expected from the latter being open-ended, except those for
218 Greenland under SSP1-26: too few Greenland simulations were performed under low
219 scenarios (RCP2.6, SSP1-26) to constrain the emulator variance (see Fig. 1a; Methods:
220 'Parameter interactions').

221

222 Emulation allows us to additionally assess the sensitivity of projections to uncertainties in
223 their inputs as well as their robustness. If we use CMIP6 global climate models for the
224 projections (Extended Data Figure 3), instead of FaIR, we find a slight increase in sea level
225 contributions due to the larger proportion of models with high climate sensitivity to carbon
226 dioxide^{33,34}: the 95th percentile increases by 7 cm under SSP5-85. We estimate the potential
227 impact of reducing uncertainty with future knowledge by using fixed values for temperature,
228 or for the ice sheet retreat and basal melt parameters: the width of the 5-95% ranges reduce
229 by up to 13% and 17% respectively (tests 2-4 in Methods: Sensitivity tests; Extended Data
230 Table 3 and Extended Data Figure 4). In other words, the ice-ocean interface is a similar
231 magnitude contributor to, or larger, uncertainty for these projections as global warming under
232 a particular emissions scenario. When we assess the robustness of the projections to different
233 selections and treatments of the ice sheet simulations, we find this makes very little
234 difference (tests 2-4 in Methods: Robustness checks; Extended Data Table 4; Extended Data
235 Figure 5).

236

237 **Antarctic focus**

238

239 No clear dependence on emissions scenario emerges for Antarctica. This is partly due to the
240 opposite scenario-dependencies of West and East Antarctica regions (Fig. 3f and g). But the
241 average response to emissions scenario for each region is also small. A key reason is the wide
242 variety of changes in the atmosphere and ocean in the global climate models. Figure 4 shows
243 ice sheet model simulations where both the high and low emissions scenario were run (two
244 climate models for Greenland, three for Antarctica). For the Greenland ice sheet, all
245 simulations predict increased mass loss under higher emissions (Fig. 4a: red shaded region).
246 For Antarctica, the picture is more complex, and mostly clustered according to the climate
247 model. Many West Antarctica simulations show the same straightforward response as
248 Greenland (Fig. 4b), particularly those that do not use the ISMIP6 basal melting
249 parameterisation (see Methods). However, the West Antarctica simulations driven by
250 CNRM-CM6-1 show the reverse, where mass gain through snowfall accumulation increases
251 more under high emissions than mass loss (which is predominantly ocean-induced). (Note
252 fewer simulations were driven by IPSL-CM5A-MR and CNRM-CM6-1 than by NorESM1-
253 M, so their spread is necessarily smaller). East Antarctica and the Peninsula mostly also show
254 this latter response, though some simulations show other combinations: more mass loss under
255 low emissions than high, or mass loss under low emissions and mass gain under high.
256

257 It is challenging to evaluate which of these three climate models, or others used by ISMIP6,
258 are most reliable for Antarctic climate change. Ocean conditions and accumulation show
259 large spatio-temporal variability and are sparsely observed; models imperfectly represent
260 important processes, and it is unclear whether the newer CMIP6 models have improved
261 relative to CMIP5^{13,35-38}. Most of the climate models were from CMIP5, including
262 NorESM1-M and IPSL-CM5A-MR, and were selected by their success at reproducing
263 southern climatological observations (while also sampling a range of future climate
264 responses)¹⁸. NorESM-1M has a lower than average atmospheric warming, hence less
265 snowfall, while IPSL-CM5A-MR is higher than average (particularly for East Antarctica)¹⁸.
266 The newer CMIP6 models, including CNRM-CM6-1, were selected only by their availability.
267 Changing the selection or treatment of Antarctica simulations – e.g. using subsets of climate
268 models, or rejecting simulations with net mass gain early in the projections – do not result in
269 any substantial scenario-dependence (see tests 7-10 in Methods: Robustness checks;
270 Extended Data Table 4; Extended Data Figure 5).

271

272 Uncertainty about the scenario-dependence of Antarctic projections is not new. The IPCC
273 Fifth Assessment Report (2013) stated 'the current state of knowledge does not permit an
274 assessment' of the dependence of rapid dynamical change on scenario. Some studies that
275 show strong scenario-dependence neglect the compensating accumulation part^{26,39}, use
276 extreme¹ ice shelf collapse scenarios²⁴, or the basal melt parameterisation uncertainty is the
277 same order as, or larger than, the scenario-dependence^{27,40,41}. To be clear, we do not assert
278 that Antarctica's future does not depend on future greenhouse emissions or global warming:
279 only that the relationship between global and Antarctic climate change, and the ice sheet's
280 response, are complex, only partially understood, and involve compensating factors of
281 increasing mass loss and gain which result in a balance we are not yet confident about.

282

283 We test the sensitivity of the Antarctica projections to the basal melting parameter. The main
284 projections combine two distributions¹³ for γ derived from observations of mean Antarctic
285 basal melt rates or the ten highest melt rates for Pine Island Glacier (see Methods). Using the
286 mean distribution decreases the median to ~ 0 cm SLE and the 95th percentile to ~ 8 cm SLE
287 for all scenarios; using the high distribution has less effect, increasing the median to 6 cm
288 SLE and the 95th percentile to ~ 16 cm SLE (Extended Data Table 3 and Extended Data
289 Figure 4: tests 5 and 6). We also try and reproduce the higher projections of ref. [26] using a
290 similar approach to sampling basal melt (see Methods), and find we only obtain similar
291 projections when using extreme values of our parameter range (Extended Data Table 3 and
292 Extended Data Figure 4: tests 7 and 8). This suggests ref. [26] could be interpreted as more
293 pessimistic projections: they use values of basal melt sensitivity to ocean temperature
294 consistent with those estimated for the Amundsen Sea region³⁹, which is currently
295 undergoing most change.

296

297 However, other factors can lead to similarly high projections. In particular, the sensitivity of
298 an individual ice sheet model to the basal melt parameter can have a large effect. This differs
299 widely across ice sheet models, and also depends on the climate model (Extended Data
300 Figure 6). Emulator projections based on a single model with high or low sensitivity are
301 shown in Extended Data Figure 5 (tests 4 and 5; Extended Data Table 4). These also do not
302 show strong scenario-dependence – just a 2-3 cm decrease under high emissions for the low
303 sensitivity model, because the snowfall effect is more apparent – but instead predict a high or
304 low sea level contribution, respectively, regardless of scenario (95th percentiles: 29-30 cm
305 and 7-9 cm, respectively). The high sensitivity of the first model (SICOPOLIS) is probably

306 due to the way that sub-shelf melting is applied: over entire grid cells along the grounding
307 line, rather than just the parts detected as floating²⁶. We also show results from the four most
308 sensitive models, which are similarly high (Extended Data Table 4 and Extended Data Figure
309 5: test 6). We do not have sufficient observations to evaluate which ice sheet models have the
310 most realistic response, nor sufficient understanding to confidently predict how basal melt
311 sensitivity might change in future^{13,36}, and therefore use all models in the main projections
312 (see also 'Risk-averse projections' below).

313

314 The ice shelf collapse scenario has little effect on our projections. Switching it on increases
315 the Antarctic Peninsula and East Antarctic median contributions by 1 cm and 0-1 cm SLE
316 from 2015-2100, with no change for West Antarctica (Extended Data Table 3 and Extended
317 Data Figure 4: test 9-10). This is similar, within uncertainties, to the ice sheet simulations
318 (Extended Data Figure 7). The effect is small because surface meltwater is not projected to be
319 enough to cause collapses until the second half of the century, and even then only for small
320 number of shelves, mostly around the Peninsula¹⁵. Some combinations of climate and ice
321 sheet models do project larger sea level contributions – in particular, 5 cm for East Antarctica
322 from the SICOPOLIS ice sheet model driven by HadGEM2-ES. The HadGEM2-ES climate
323 model projects extreme ocean warming in the Ross Sea¹⁸, while SICOPOLIS has one of the
324 largest responses among the ice sheet models (as described above). If these two were found
325 to be the most realistic models, then the ISMIP6 ensemble and emulator may underestimate
326 the effect of ice shelf collapse by a few centimetres. Further results are in the Methods
327 ('Parameter interactions').

328

329 **Risk-averse projections**

330

331 Given the wide range and cancellations of responses across models and parameters, we
332 present alternative 'pessimistic but physically plausible' Antarctica projections for risk-averse
333 stakeholders, by combining a set of assumptions that lead to high sea level contributions.
334 These are: the four ice sheet models most sensitive to basal melting; the four climate models
335 that lead to highest Antarctic sea level contributions, and the one used to drive most of the ice
336 shelf collapse simulations; the high basal melt (Pine Island Glacier) distribution; and with ice
337 shelf collapse 'on' (i.e. combining robustness tests 6 and 7 and sensitivity tests 6 and 10). This
338 storyline would come about if the high basal melt sensitivities currently observed at Pine
339 Island Glacier soon become widespread around the continent; the ice sheet responds to these

340 with extensive retreat and rapid ice flow; and atmospheric warming is sufficient to
341 disintegrate ice shelves, but does not substantially increase snowfall. The risk-averse
342 projections are more than five times the main estimates: median 21 cm (95th percentile range
343 7 to 43 cm) under the NDCs (Fig. 3j), and essentially the same under SSP5-85 (Table 1;
344 regions shown in Extended Data Figure 4: test 11), with the 95th percentiles emerging above
345 the main projections after 2040 (Fig. 3d). This is very similar to projections²⁴ under an
346 extreme scenario of widespread ice shelf collapses for RCP8.5 (median 21 cm; 95th percentile
347 range 9 to 39 cm). The median is higher than ref. [26] for RCP8.5, though the 95th percentile
348 is smaller. No models that include a representation of rapid ice cliff collapse through the
349 proposed 'Marine Ice Cliff Instability'⁴³ mechanism participated in ISMIP6. This hypothesis
350 is the process with the largest estimated systematic impact on projections: it could increase
351 projections by tens of centimetres, if both the mechanism and projections of extreme ice shelf
352 collapse are found to be robust^{24,44}.

353

354 Our risk-averse Antarctica projections increase the total land ice sea level contribution to 42
355 cm (95th percentile 25 to 67 cm) SLE under current policies and pledges (NDCs), and to 30
356 cm (95th percentile 12 to 56 cm) SLE even under SSP1-19. This means that plausible
357 modelling choices for Antarctica could change the median land ice contribution by more (17
358 cm SLE) than the difference between these emissions scenarios (12 cm SLE). This ambiguity
359 limits confidence in assessing the effectiveness of mitigation on the response of global land
360 ice to climate change. When combined, the effects of uncertain emissions and Antarctic
361 response lead to a threefold spread in median projections of the land ice contribution to sea
362 level rise, ranging from 13 to 42 cm SLE over 2015-2100, implying that flexible adaptation
363 under substantial uncertainty will be essential until either can be further constrained.

364

365 Not all modelling uncertainties could be systematically assessed here. Aside from the ice cliff
366 instability hypothesis, these include ice sheet basal hydrology and sliding; glacier model
367 parameters, ice-water interactions, and meltwater routing; model initialisation; and the use of
368 coarse resolution global climate models (and a single high-resolution regional model for the
369 Greenland ice sheet). The probabilities we present are therefore specific to our ensembles,
370 and adding new climate and ice sheet models, or exploration of new parameters, could shift
371 or broaden their distributions⁴⁵. However, our projections demonstrate the importance of
372 systematic design to assess as many uncertainties as feasible, and represent the current state-
373 of-the art in estimating the land ice contribution to global mean sea level rise.

Sea level contribution from 2015-2100 (cm SLE)	Main projections		Risk-averse projections	
	50 [5, 95]% percentiles	[17, 83]% percentiles	50 [5, 95]% percentiles	[17, 83]% percentiles
Global glaciers				
SSP119	7 [4, 10]	[5, 9]		
SSP126	8 [5, 12]	[6, 10]		
SSP245	11 [7, 15]	[9, 13]		
NDCs	13 [9, 18]	[11, 16]		
SSP370	14 [10, 19]	[12, 17]		
SSP585	16 [12, 21]	[14, 19]		
Greenland ice sheet				
SSP1-19	2 [-6, 11]	[-2, 7]		
SSP1-26	3 [-4, 12]	[-1, 8]		
SSP2-45	5 [-2, 14]	[1, 10]		
NDCs	7 [0, 16]	[3, 12]		
SSP3-70	8 [0, 17]	[4, 13]		
SSP5-85	10 [2, 20]	[5, 15]		
Antarctic ice sheet				
SSP1-19	4 [-5, 14]	[-1, 10]	21 [6, 42]	[12, 32]
SSP1-26	4 [-5, 14]	[-1, 10]	21 [7, 43]	[12, 31]
SSP2-45	4 [-5, 14]	[-1, 9]	21 [7, 43]	[12, 31]
NDCs	4 [-5, 14]	[-1, 10]	21 [7, 43]	[13, 31]
SSP3-70	4 [-5, 14]	[-1, 10]	21 [8, 43]	[13, 31]
SSP5-85	4 [-5, 14]	[-1, 10]	22 [8, 43]	[14, 32]
Land ice				
SSP1-19	13 [0, 28]	[6, 21]	30 [12, 56]	[20, 43]
SSP1-26	16 [3, 30]	[8, 24]	33 [15, 58]	[22, 45]
SSP2-45	20 [7, 35]	[13, 28]	38 [20, 63]	[28, 50]
NDCs	25 [11, 40]	[17, 33]	42 [25, 67]	[32, 54]
SSP3-70	27 [13, 41]	[19, 35]	44 [27, 70]	[34, 56]
SSP5-85	30 [16, 46]	[22, 39]	48 [30, 75]	[38, 61]

374

375 **Acknowledgements**

376 We thank Jonathan Rougier for generously providing advice and support throughout, and
377 writing the original random effects model. We also thank Baylor Fox-Kemper, Helene
378 Hewitt, Robert Kopp, Sybren Drijfhout and Jeremy Rohmer for useful discussions,
379 suggestions and support. We thank Daniel Williamson, Nicholas Barrand and two
380 anonymous referees for their thorough and constructive comments, which greatly improved
381 the manuscript. We thank the Climate and Cryosphere (CliC) effort, which provided support
382 for ISMIP6 and GlacierMIP through sponsoring of workshops, hosting the websites and
383 ISMIP6 wiki, and promotion. We acknowledge the World Climate Research Programme,
384 which, through its Working Group on Coupled Modelling, coordinated and promoted CMIP5
385 and CMIP6. We thank the climate modeling groups for producing and making available their
386 model output, the Earth System Grid Federation (ESGF) for archiving the CMIP data and
387 providing access, the University at Buffalo for ISMIP6 data distribution and upload, and the
388 multiple funding agencies who support CMIP5 and CMIP6 and ESGF. We thank the ISMIP6
389 steering committee, the ISMIP6 model selection group and the ISMIP6 dataset preparation
390 group for their continuous engagement in defining ISMIP6. This is ISMIP6 contribution No.
391 13. This publication was supported by PROTECT, which has received funding from the
392 European Union's Horizon 2020 research and innovation programme under grant agreement
393 No 869304. This is PROTECT contribution number XX.

394

395 Individual author acknowledgements follow. Tamsin Edwards was supported by PROTECT
396 and the UK Natural Environment Research Council grant NE/T007443/1. Fiona Turner was
397 supported by PROTECT. James O'Neill was supported by the UK Natural Environment
398 Research Council London Doctoral Training Partnership. Rupert Gladstone's contribution
399 was supported by Academy of Finland grants 286587 and 322430. William Lipscomb and
400 Gunter Leguy were supported by the National Center for Atmospheric Research, which is a
401 major facility sponsored by the National Science Foundation under Cooperative Agreement
402 No. 1852977. Computing and data storage resources for CISM simulations, including the
403 Cheyenne supercomputer (doi:10.5065/D6RX99HX), were provided by the Computational
404 and Information Systems Laboratory (CISL) at NCAR. Support for Xylar Asay-Davis,
405 Matthew J. Hoffman, Stephen Price, and Tong Zhang was provided through the Scientific
406 Discovery through Advanced Computing (SciDAC) program funded by the US Department

407 of Energy (DOE), Office of Science, Advanced Scientific Computing Research and
408 Biological and Environmental Research Programs. Nicholas R. Golledge, Daniel P. Lowry
409 and Brian Anderson were supported by NZ Ministry for Business, Innovation and
410 Employment contracts RTUV1705 ('NZSeaRise') and ANTA1801 ('Antarctic Science
411 Platform'). Jonathan Gregory and Robin S. Smith were supported by the National Centre for
412 Atmospheric Science, funded by the UK National Environment Research Council. Reinhard
413 Calov was funded by the PalMod project of the Bundesministerium für Bildung und
414 Forschung (BMBF) with the grants FKZ 01LP1502C and 01LP1504D. Daniel Martin and
415 Courtney Shafer were supported by the Director, Office of Science, Offices of Advanced
416 Scientific Computing Research (ASCR) and Biological and Environmental Research (BER),
417 of the U.S. Department of Energy under Contract No. DE-AC02-05CH11231, as a part of the
418 ProSPect SciDAC Partnership. BISICLES simulations used resources of the National Energy
419 Research Scientific Computing Center (NERSC), a U.S. Department of Energy Office of
420 Science User Facility operated under Contract No. DE-AC02-05CH11231. Chen Zhao and
421 Ben Galton-Fenzi were supported under the Australian Research Council's Special Research
422 Initiative for Antarctic Gateway Partnership (Project ID SR140300001) and received grant
423 funding from the Australian Government for the Australian Antarctic Program Partnership
424 (Project ID ASCI000002). Work was performed by Eric Larour, Nicole Schlegel, and Helene
425 Seroussi at the California Institute of Technology's Jet Propulsion Laboratory under a
426 contract with the National Aeronautics and Space Administration's Cryosphere, Sea Level
427 Change Team, and Modeling, Analysis and Prediction (MAP) Programs. They acknowledge
428 computational resources and support from the NASA Advanced Supercomputing Division.
429 The CMIP5 and CMIP6 projection data were processed by Christine McKenna with funding
430 from the European Union's CONSTRAIN project as part of the Horizon 2020 Research and
431 Innovation Programme under grant agreement number 820829. Alice Barthel was supported
432 by the DOE Office of Science HiLAT-RASM project and Early Career Research program.
433 Helene Seroussi was supported by grants from NASA Cryospheric Science, Sea Level
434 Change Team, and Modeling, Analysis, and Predictions Programs. Torsten Albrecht and
435 Ricarda Winkelmann are supported by the Deutsche Forschungsgemeinschaft (DFG) in the
436 framework of the priority program "Antarctic Research with comparative investigations in
437 Arctic ice areas" by grants WI4556/2-1 and WI4556/4-1, and within the framework of the
438 PalMod project (FKZ: 01LP1925D) supported by the German Federal Ministry of Education
439 and Research (BMBF) as a Research for Sustainability initiative (FONA). Ronja Reese is

440 supported by the Deutsche Forschungsgemeinschaft (DFG) by grant WI4556/3-1 and through
441 the TiPACCs project that receives funding from the European Union's Horizon 2020
442 Research and Innovation program under grant agreement no. 820575. Ralf Greve and
443 Christopher Chambers were supported by Japan Society for the Promotion of Science (JSPS)
444 KAKENHI grant Nos. JP16H02224 and JP17H06323. Ralf Greve was supported by JSPS
445 KAKENHI grant No. JP17H06104, by a Leadership Research Grant of Hokkaido
446 University's Institute of Low Temperature Science (ILTS), and by the Arctic Challenge for
447 Sustainability (ArCS) project of the Japanese Ministry of Education, Culture, Sports, Science
448 and Technology (MEXT) (program grant number JPMXD1300000000). Frank Pattyn and
449 Sainan Sun were supported by the MIMO project within the STEREO III programme of the
450 Belgian Science Policy Office, contract SR/00/336 and the Fonds de la Recherche
451 Scientifique (FNRS) and the Fonds Wetenschappelijk Onderzoek-Vlaanderen (FWO) under
452 the EOS Project number O0100718F. Andrew Shepherd was supported by the UK Natural
453 Environment Research Council in partnership with the Centre for Polar Observation and
454 Modelling and the British Antarctic Survey and by the European Space Agency Climate
455 Change Initiative. Denis Felikson was supported by an appointment to the NASA
456 Postdoctoral Program at the NASA Goddard Space Flight Center, administered by
457 Universities Space Research Association under contract with NASA.

458

459 **Author contributions**

460

461 T.L.E. conceived the idea, carried out all statistical analysis except the random effects model,
462 produced the figures, and wrote the manuscript. S.N. led ISMIP6, including experimental
463 design, organisation and analysis, and provided scientific interpretation. B.M and R.H. co-led
464 GlacierMIP and contributed simulations (below), and provided data and interpretation. H. G.
465 and H.S. led the processing and analysis in ISMIP6 for the Greenland and Antarctic ice
466 sheets, respectively, contributed simulations (below), and provided scientific interpretation
467 and advice. N.J. and D.S. co-derived with T.L.E. the ice sheet continuous parameter
468 distributions for the emulator, and also derived the corresponding ocean forcing
469 parameterisation studies with X.A.-D. and T.H. for Antarctica and F.S., D.F. and M.M. for
470 Greenland. F.T. performed the random effects model cross-check for Antarctica. C.S.
471 provided the FaIR projections and C.M. provided the CMIP5 and CMIP6 projection data for
472 the emulator. E.S. led the ISMIP6 data processing. A.A.O., J.M.G., E.L., W.H.L., A.J.P.,

473 A.S. contributed to the ISMIP6 experimental design, organisation and analysis as members of
474 its steering committee, and R.S and W.H.L. led the ISMIP6 atmosphere focus group. C.M.L.,
475 A.B. and C.A. selected the CMIP5 models for ISMIP6, X.F. and P.A. ran the surface mass
476 balance model for the Greenland and R.Cu. prepared the Antarctic surface mass balance, and
477 L.D.T. and M.v.d.B. provided the ice shelf collapse forcing. For Antarctica: T.K. and A.H.
478 contributed the AWI/PISM simulations; M.H., T.Z. and S.P. contributed the DOE/MALI
479 simulations; R.G. and R.Ca. contributed the ILTS_PIK/SICOPOLIS simulations; H.G. and
480 R.v. d. W. contributed the IMAU/IMAUICE simulations; N.-J.S. and H.S. contributed the
481 JPL/ISSM simulations; C.D. and A.Q. contributed the LSCE/GRISLI simulations; G.L. and
482 W.L. contributed the NCAR/CISM simulations; R.R., T.A. and R.W. contributed the
483 PIK/PISM simulations;. T.P., M.M. and H.S. contributed the UCIJPL/ISSM simulations; F.P.
484 and S.S. contributed the ULB/fETISH simulations; C.Z., R.G., B.G-F. and T.Z. contributed
485 the UTAS/Elmer/Ice simulations; J.V.B. and P.H. contributed the VUB/AISMPALEO
486 simulations; N.R.G. and D.L. contributed the VUW/PISM simulations; and D.F.M. and C.S.
487 contributed the CPOM/BISICLES simulations. For Greenland: M.R. and A.H. contributed
488 the AWI/ISSM simulations; V.L. and A.J.P. contributed the BGC/BISICLES simulations;
489 I.N., D.F. and S.N. contributed the GSFC/ISSM simulations; R.G., R.Ca. and C.C.
490 contributed the ILTS_PIK/SICOPOLIS simulations; H.G., R.v.d.W. and M.v.d.B. contributed
491 the IMAU/IMAUICE simulations; N.-J.S. and H.S. contributed the JPL/ISSM simulations;
492 J.C. and N.-J.S. contributed the JPL/ISSMPALEO simulations; A.Q. and C.D. contributed
493 the LSCE/GRISLI simulations; L.T. contributed the MUN/GSM simulations; W.H.L. and
494 G.R.L. contributed the NCAR/CISM simulations; A.A contributed the UAF/PISM
495 simulations; Y.C., H.S. and M.M. contributed the UCIJPL/ISSM simulations; S.L.c. and P.H.
496 contributed the VUB/GISM simulations; and D.P.L. and N.R.G. contributed the VUW/PISM
497 simulations. For global glaciers: B.A. contributed the AND2012 simulations; K.F. and A.S.
498 contributed the GLIMB simulations; M.H. contributed the GloGEM simulations; H.Z.
499 contributed the GloGEMflow simulations; S.S. contributed the JULES simulations; P.K. and
500 W.I. contributed the KRA2017 simulations; B.M. and J.M. contributed the MAR2012
501 simulations; F.M. and N.C. contributed the OGGM simulations; D.R. and R.H. contributed
502 the PyGEM simulations; A.B. and V.R. contributed the RAD2014 simulations; R.v.d.W.
503 contributed the WAL2001 simulations; and A. Bl. and J.-H. M. assisted with data handling.
504 All authors contributed to the manuscript.

505

506 References

- 507
- 508 1. Oppenheimer, M. *et al.* in *IPCC Special Report on the Ocean and Cryosphere in a*
509 *Changing Climate* (eds. Portner, H. O. *et al.*) (2019).
- 510 2. Nowicki, S. M. J. *et al.* Ice Sheet Model Intercomparison Project (ISMIP6)
511 contribution to CMIP6. *Geoscientific Model Development* 9, 4521–4545 (2016).
- 512 3. Nowicki, S. *et al.* Experimental protocol for sea level projections from ISMIP6 stand-
513 alone ice sheet models. *The Cryosphere*, 14, 2331–2368, [https://doi.org/10.5194/tc-14-](https://doi.org/10.5194/tc-14-2331-2020)
514 [2331-2020](https://doi.org/10.5194/tc-14-2331-2020), 2020.
- 515 4. Eyring, V. *et al.* Overview of the Coupled Model Intercomparison Project Phase 6
516 (CMIP6) experimental design and organization. *Geoscientific Model Development* 9,
517 1937–1958 (2016).
- 518 5. Hock, R. *et al.* GlacierMIP – A model intercomparison of global-scale glacier mass-
519 balance models and projections. *Journal of Glaciology* 65, 453–467 (2019).
520 <https://doi.org/10.1017/jog.2019.22>
- 521 6. Goelzer, H. *et al.* Design and results of the ice sheet model initialisation experiments
522 initMIP-Greenland: an ISMIP6 intercomparison. *The Cryosphere* 12, 1433–1460
523 (2018).
- 524 7. Seroussi, H. *et al.* initMIP-Antarctica: an ice sheet model initialization experiment of
525 ISMIP6. *The Cryosphere* 13, 1441–1471 (2019).
- 526 8. Marzeion, B. *et al.* Partitioning the Uncertainty of Ensemble Projections of Global
527 Glacier Mass Change. *Earth's Future*, 8(7), e2019EF001470 (2020).
- 528 9. van Vuuren, D. P. *et al.* The representative concentration pathways: an overview.
529 *Climatic Change* 109, 5–31 (2011).
- 530 10. Slater, D. A. *et al.* Estimating Greenland tidewater glacier retreat driven by submarine
531 melting. *The Cryosphere* 13, 2489–2509 (2019).
- 532 11. Slater, D. A. *et al.* Twenty-first century ocean forcing of the Greenland ice sheet for
533 modelling of sea level contribution, *The Cryosphere*, 14, 985–1008,
534 <https://doi.org/10.5194/tc-14-985-2020>, 2020.
- 535 12. Favier, L. *et al.* Assessment of sub-shelf melting parameterisations using the ocean–
536 ice-sheet coupled model NEMO(v3.6)–Elmer/Ice(v8.3). *Geoscientific Model*
537 *Development* 12, 2255–2283 (2019).
- 538 13. Jourdain, N. C. *et al.* A protocol for calculating basal melt rates in the ISMIP6
539 Antarctic ice sheet projections, *The Cryosphere*, 14, 3111–3134,
540 <https://doi.org/10.5194/tc-14-3111-2020>, 2020.
- 541 14. Goelzer, H. *et al.* The future sea-level contribution of the Greenland ice sheet: a multi-
542 model ensemble study of ISMIP6. *The Cryosphere*, 14, 3071–3096,
543 <https://doi.org/10.5194/tc-14-3071-2020> (2020).
- 544 15. Seroussi, H. *et al.* ISMIP6 Antarctica: a multi-model ensemble of the Antarctic ice
545 sheet evolution over the 21st century. *The Cryosphere*, 14, 3033–3070,
546 <https://doi.org/10.5194/tc-14-3033-2020> (2020).
- 547 16. Nowicki, S. *et al.* Contrasting contributions to future sea level under CMIP5 and
548 CMIP6 scenarios from the Greenland and Antarctic ice sheets. *Geophysical Research*
549 *Letters*, in review.
- 550 17. Goelzer, H. *et al.* Remapping of Greenland ice sheet surface mass balance anomalies
551 for large ensemble sea-level change projections. *The Cryosphere*, 14, 1747–1762,
552 <https://doi.org/10.5194/tc-14-1747-2020>, 2020.
- 553 18. Barthel, A. *et al.* CMIP5 model selection for ISMIP6 ice sheet model forcing:
554 Greenland and Antarctica, *The Cryosphere*, 14, 855–879, [https://doi.org/10.5194/tc-](https://doi.org/10.5194/tc-14-855-2020)
555 [14-855-2020](https://doi.org/10.5194/tc-14-855-2020), 2020.

- 556 19. Riahi, K. *et al.* The Shared Socioeconomic Pathways and their energy, land use, and
557 greenhouse gas emissions implications: An overview. *Global Environmental Change*
558 42, 153–168 (2017).
- 559 20. O'Neill, B. C. *et al.* The Scenario Model Intercomparison Project (ScenarioMIP) for
560 CMIP6. *Geoscientific Model Development* 9, 3461–3482 (2016).
- 561 21. Taylor, K. E., Stouffer, R. J. & Meehl, G. A. An Overview of CMIP5 and the
562 Experiment Design. *B Am Meteorol Soc* 93, 485–498 (2012).
- 563 22. Andrianakis, I. & Challenor, P. G. The effect of the nugget on Gaussian process
564 emulators of computer models. *Computational Statistics & Data Analysis* 56, 4215–
565 4228 (2012).
- 566 23. Gramacy, R. B. & Lee, H. K. H. Cases for the nugget in modeling computer
567 experiments. *Stat Comput* 22, 713–722 (2010).
- 568 24. Edwards, T. L. *et al.* Revisiting Antarctic ice loss due to marine ice cliff instability.
569 *Nature* 566, 58–64 (2019).
- 570 25. Church, J.A., P.U. Clark, A. Cazenave, J.M. Gregory, S. Jevrejeva, A. Levermann,
571 M.A. Merrifield, G.A. Milne, R.S. Nerem, P.D. Nunn, A.J. Payne, W.T. Pfeffer, D.
572 Stammer and A.S. Unnikrishnan, 2013: Sea Level Change. In: *Climate Change 2013:*
573 *The Physical Science Basis. Contribution of Working Group I to the Fifth Assessment*
574 *Report of the Intergovernmental Panel on Climate Change* [Stocker, T.F., D. Qin, G.-
575 K. Plattner, M. Tignor, S.K. Allen, J. Boschung, A. Nauels, Y. Xia, V. Bex and P.M.
576 Midgley (eds.)]. Cambridge University Press, Cambridge, United Kingdom and New
577 York, NY, USA.
- 578 26. Levermann, A. *et al.* Projecting Antarctica's contribution to future sea level rise from
579 basal ice shelf melt using linear response functions of 16 ice sheet models (LARMIP-
580 2). *Earth Syst. Dynam.* 11, 35–76 (2020).
- 581 27. Bulthuis, K. *et al.*, Uncertainty quantification of the multi-centennial response of the
582 Antarctic ice sheet to climate change, *The Cryosphere*, 13, 1349–1380,
583 <https://doi.org/10.5194/tc-13-1349-2019>, 2019.
- 584 28. Nauels, A. *et al.*, Synthesizing long-term sea level rise projections – the MAGICC sea
585 level model v2.0. *Geosci. Model Dev.*, 10, 2495–2524 (2017)
- 586 29. Palmer, M. D., *et al.* (2020). Exploring the drivers of global and local sea-level change
587 over the 21st century and beyond. *Earth's Future*, 8, e2019EF001413. [https://doi.org/](https://doi.org/10.1029/2019EF001413)
588 [10.1029/2019EF001413](https://doi.org/10.1029/2019EF001413)
- 589 30. McKenna, C. M. *et al.*, Stringent mitigation substantially reduces risk of unprecedented
590 near-term warming rates, *Nature Climate Change*, in press.
- 591 31. Farinotti, D. *et al.*, A consensus estimate for the ice thickness distribution of all
592 glaciers on Earth, *Nature Geoscience*, 12, 168–173 (2019).
- 593 32. Biemans *et al.* (2019) Importance of snow and glacier meltwater for agriculture on the
594 Indo-Gangetic Plain, *Nature Sustainability* 2, 594–601
- 595 33. Forster, P. M., Maycock, A. C., McKenna, C. M. & Smith, C. J. Latest climate models
596 confirm need for urgent mitigation. *Nature Climate Change* 1–4 (2019).
597 doi:10.1038/s41558-019-0660-0
- 598 34. Meehl, G. *et al.* (2020) Context for interpreting equilibrium climate sensitivity and
599 transient climate response from the CMIP6 Earth system models, *Sci. Adv.*, 6 :
600 eaba1981
- 601 35. Meredith, M. *et al.* in *IPCC Special Report on the Ocean and Cryosphere in a*
602 *Changing Climate* (eds. Portner, H. O. *et al.*) (2019).
- 603 36. Naughten, K. A. *et al.* Future Projections of Antarctic Ice Shelf Melting Based on
604 CMIP5 Scenarios. *J Climate* 31, 5243–5261 (2018).

- 605 37. Mottram, R., Hansen, N., Kittel, C., van Wessem, M., Agosta, C., Amory, C., Boberg,
606 F., van de Berg, W. J., Fettweis, X., Gossart, A., van Lipzig, N. P. M., van Meijgaard,
607 E., Orr, A., Phillips, T., Webster, S., Simonsen, S. B., and Souverijns, N.: What is the
608 Surface Mass Balance of Antarctica? An Intercomparison of Regional Climate Model
609 Estimates, *The Cryosphere Discuss.*, <https://doi.org/10.5194/tc-2019-333>, in review,
610 2020.
- 611 38. Roussel, M.-L., Lemonnier, F., Genthon, C., and Krinner, G.: Brief communication:
612 Evaluating Antarctic precipitation in ERA5 and CMIP6 against CloudSat observations,
613 *The Cryosphere*, 14, 2715–2727, <https://doi.org/10.5194/tc-14-2715-2020>, 2020.
- 614 39. Reese, R. *et al.*, The role of history and strength of the oceanic forcing in sea level
615 projections from Antarctica with the Parallel Ice Sheet Model, *The Cryosphere*, 14,
616 3097–3110, <https://doi.org/10.5194/tc-14-3097-2020>, 2020.
- 617 40. Golledge, N. R. *et al.* The multi-millennial Antarctic commitment to future sea-level
618 rise. *Nature* **526**, 421–425 (2015).
- 619 41. Golledge, N. R. *et al.* Global environmental consequences of twenty-first-century ice-
620 sheet melt. *Nature Publishing Group* 1–23 (2019). doi:10.1038/s41586-019-0889-9
- 621 42. Levermann, A. *et al.* Projecting Antarctica's contribution to future sea level rise from
622 basal ice shelf melt using linear response functions of 16 ice sheet models (LARMIP-
623 2). *Earth Syst. Dynam.* 11, 35–76 (2020).
- 624 43. DeConto, R. M. & Pollard, D. Contribution of Antarctica to past and future sea-level
625 rise. *Nature* 531, 591–597 (2016).
- 626 44. Clerc, F., Minchew, B. M. & Behn, M. D. Marine Ice Cliff Instability Mitigated by
627 Slow Removal of Ice Shelves. *Geophysical Research Letters* 46, 12108–12116 (2019).
- 628 45. Williamson, D. B., Sansom, P. G. (2020) How are emergent constraints quantifying
629 uncertainty and what do they leave behind? *BAMS*, 100, 2571-2588,
630 <https://doi.org/10.1175/BAMS-D-19-0131.1>
631

632 **Figure 1. Ice sheet and glacier mass loss generally increases linearly with global mean**
633 **temperature.** Projected mass changes from 2015-2100 in sea level equivalent (SLE) as a function of
634 global mean surface air temperature change over the same period for (a) Greenland ice sheet, (b, c)
635 West and East Antarctic ice sheets, (d) Greenland peripheral glaciers, (e, f) the Antarctic Peninsula
636 and Antarctic peripheral glaciers, (g-j) four glacier regions with large maximum sea level
637 contributions (Alaska, Arctic Canada North and South, Russian Arctic), (k, l) two regions with
638 nonlinear temperature-dependence and total or near-total disappearance projected at high
639 temperatures (Central Europe and Caucasus); and (m-o) three regions comprising High Mountain
640 Asia. Central solid lines show the emulator mean, and shaded regions the mean \pm 2 s.d.. For the ice
641 sheets (a-c, e), darker shaded regions use parameter values fixed at their default values (Greenland
642 glacier retreat: median; Antarctic sub-shelf basal melting: median of Mean Antarctic distribution;
643 Antarctic ice shelf collapse off), and lighter shaded regions use alternative values (Greenland: 75th
644 percentile; Antarctica: median of Pine Island Glacier distribution). See Methods for details. Points
645 show ice sheet and glacier simulations under RCP2.6/SSP1-26 (blue), RCP4.5 (yellow), RCP6.0
646 (orange) and RCP8.5/SSP5-85 (red). Solid circles for the ice sheets use the default ice-ocean
647 parameter value and open circles use the alternative value (other simulations are not shown). Glacier

648 simulations are change in total volume, not volume above flotation; the estimated maximum sea level
649 contribution (i.e. current total glacier volume above flotation)³¹ is shown (horizontal dashed line).

650

651 **Figure 2. Ice sheet mass loss strongly depends on ice-ocean parameters.** Projections of sea level
652 contribution from 2015-2100 as a function of (a) Greenland glacier retreat parameter (κ), and basal
653 melt parameter (γ) for (b) West Antarctica, (c) East Antarctica, (d) Peninsula. Solid line shows
654 emulator mean estimate using fixed global temperature (projected by the global climate model most
655 used for simulations, under RCP8.5), and shaded regions show the mean \pm 2 s.d. Symbols show ice
656 sheet models forced by this climate model for which simulations for at least three (Greenland) or four
657 (Antarctic) melt parameter values were available: circles use the ISMIP6 parameterisation for the ice-
658 ocean interface; crosses use other representations, and are assigned ensemble mean values of the
659 parameter; triangles show the Greenland ice sheet model for which two additional values of κ were
660 run.

661

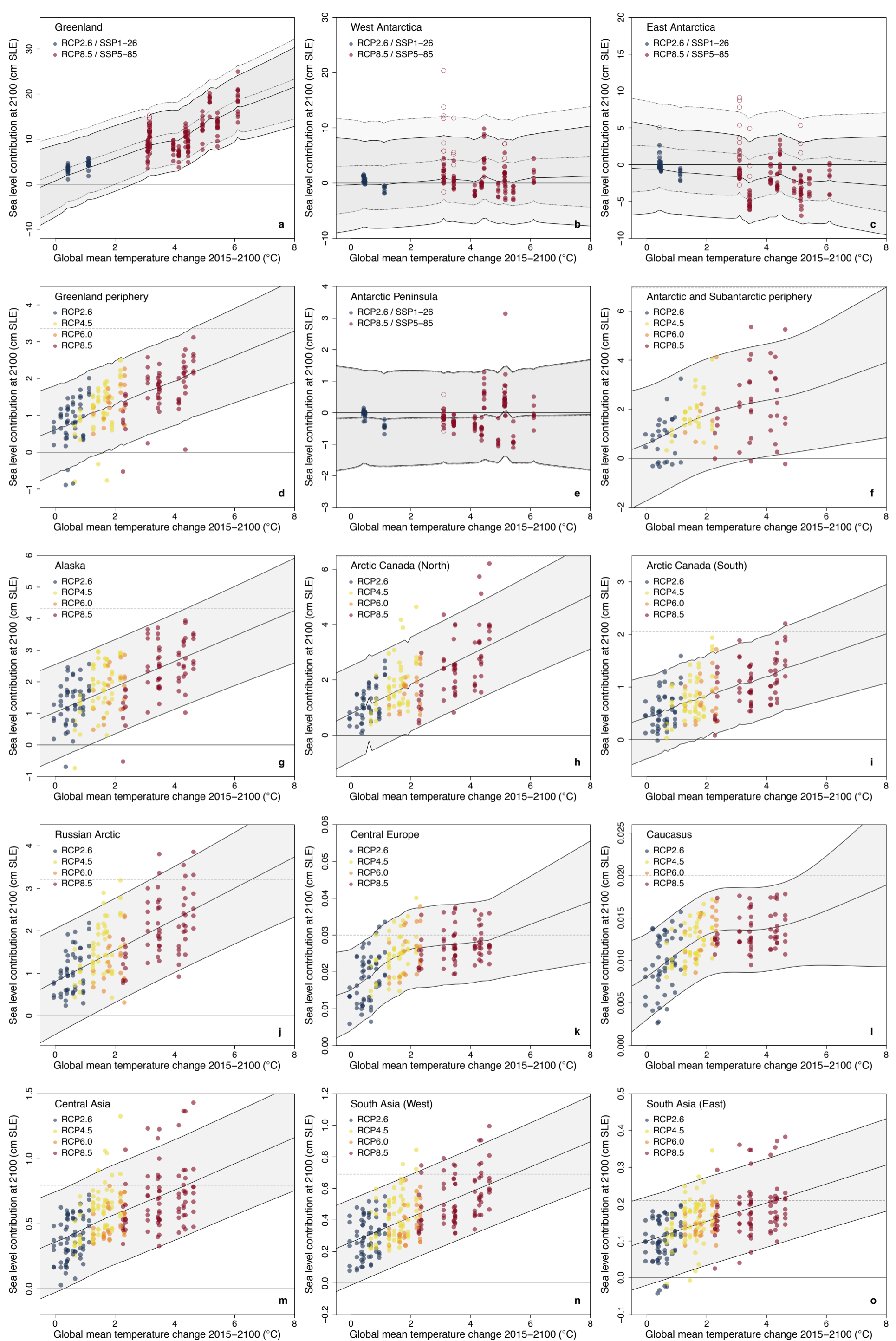
662 **Figure 3. Projected land ice contribution to 21st century sea level rise and for selected regions at**
663 **2100.** (a) Probability distributions for global mean surface air temperature change from 2015-2100
664 from the FaIR simple climate model under the five Shared Socioeconomic Pathways (SSPs) and
665 current Nationally Determined Contributions (NDCs) (N = 5000 each). (b) Greenland ice sheet retreat
666 parameter (κ) distribution (N = 10,000): vertical lines show the five values used for simulations:
667 median (solid), 25th and 75th percentiles (dashed), and 5th and 95th percentiles (dotted). (c) Antarctic
668 basal melt parameter (γ) distribution (N = 8200): vertical lines show the six values used for
669 simulations: median (solid), 5th and 95th percentiles (dashed) of the Mean Antarctic (black) and Pine
670 Island Glacier (grey) distributions (see Methods). (d) Projected land ice contribution to sea level (cm
671 SLE) from 2015-2100 under the five SSPs and NDCs. Solid lines and shaded regions: median and 5-
672 95th percentiles (N = 11,500 per year per scenario): 5 year smoothing applied, with original data
673 shown as dots (interannual variation arises from annual sampling of emulator uncertainties). Pale
674 solid lines: 95th percentiles of risk-averse projections. Box and whiskers show [5, 25, 50, 75, 95]th
675 percentiles at 2100 (N = 115,000 per scenario) for main projections (left) and risk-averse projections
676 for Antarctica (right). (e-j). Probability density functions for 2100 estimated for: (e) Greenland ice
677 sheet, (f) Arctic Canada North, (g) total for glaciers, (h, i) West and East Antarctica for all scenarios,
678 and (j) total for Antarctic ice sheet under main and risk-averse projections for the NDCs. Glacier and
679 Antarctic totals are less smooth because they are estimated from a sum of Monte Carlo samples from
680 each region, rather than deterministic integration (see Methods); these samples are shown for SSP1-19
681 and NDCs (N = 5000). Ice sheet projections do not include pre-2015 response, which is estimated to
682 add less than 1 cm to the Greenland contribution and up to ~2 cm to the Antarctic (see Methods).

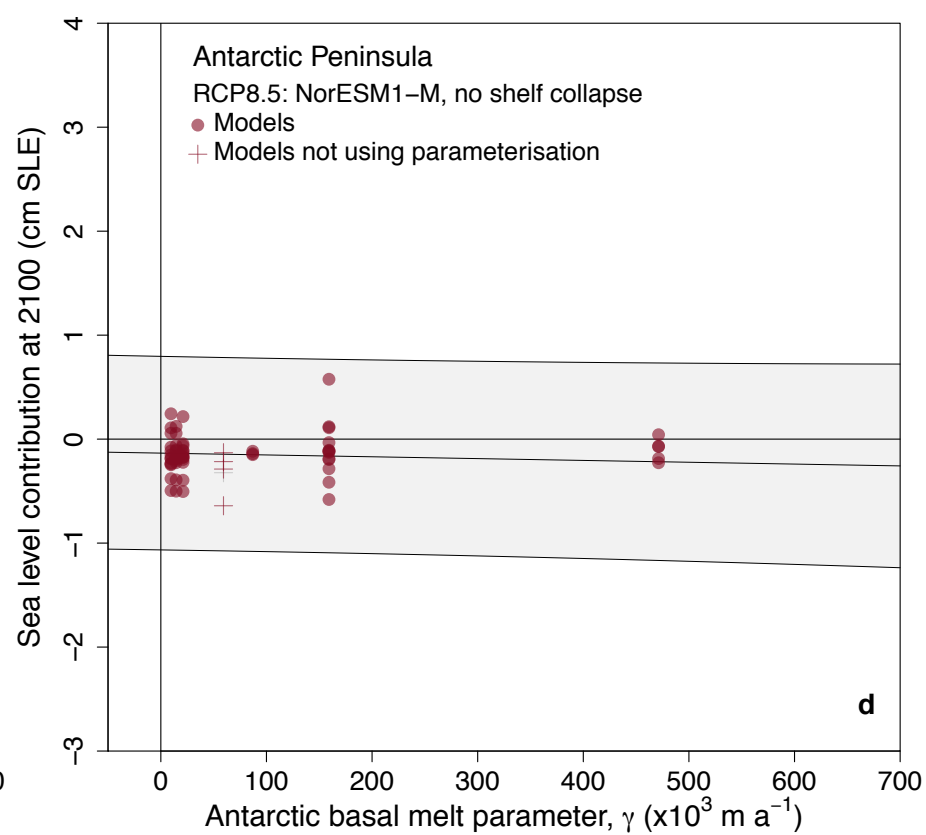
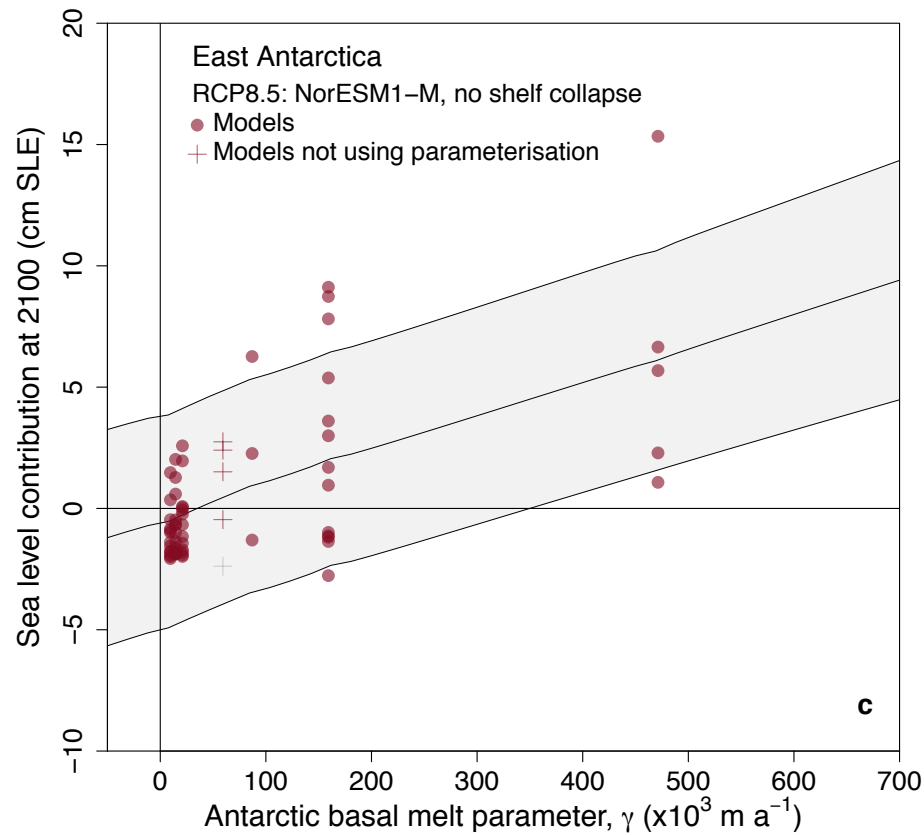
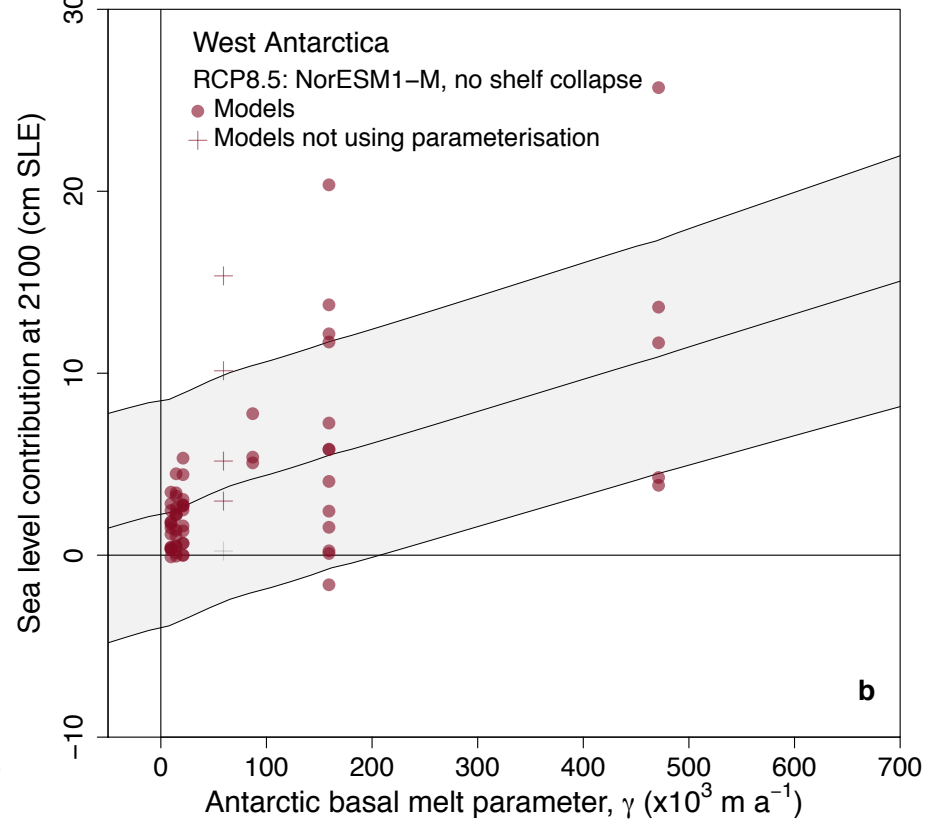
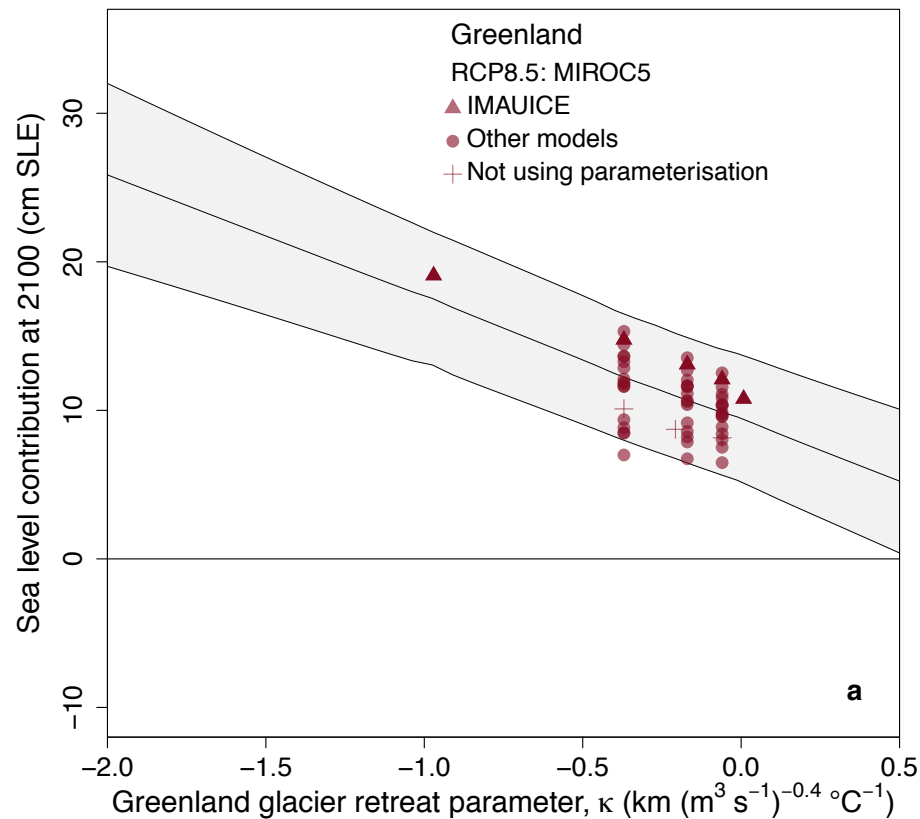
683

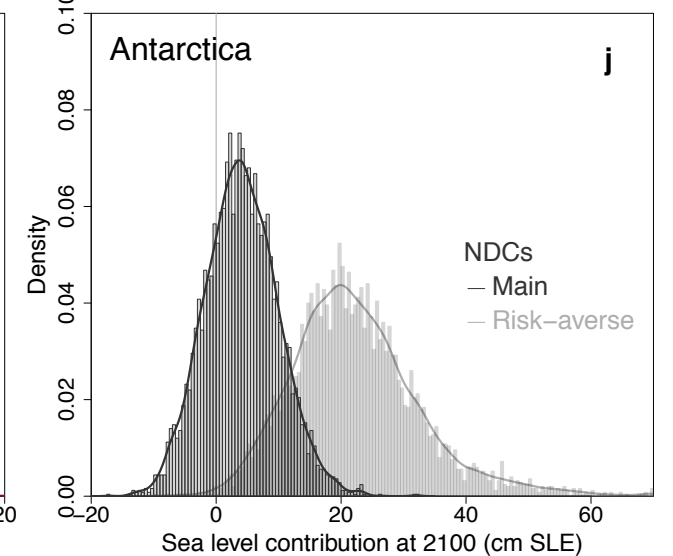
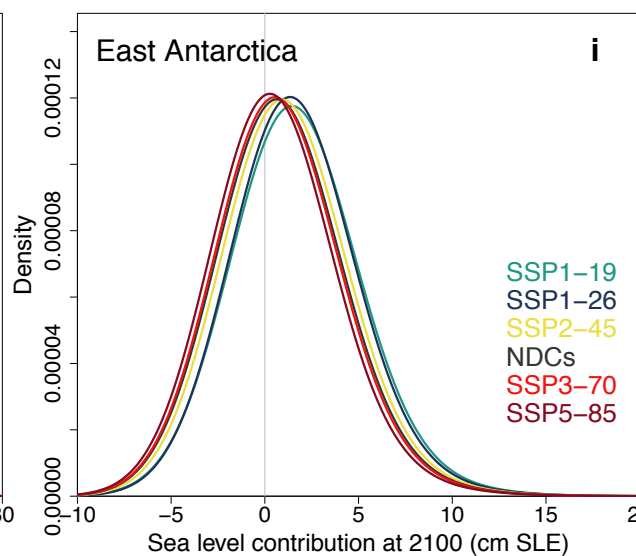
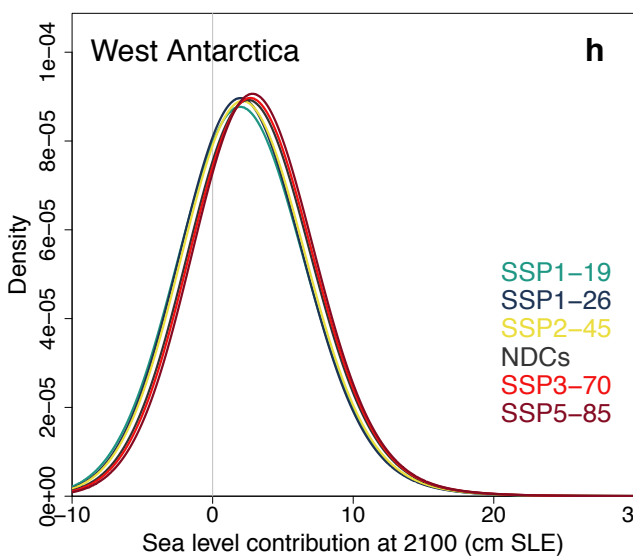
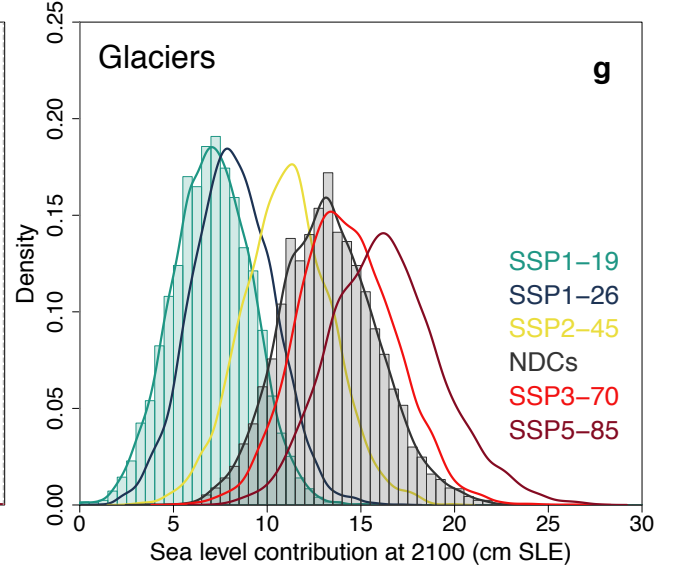
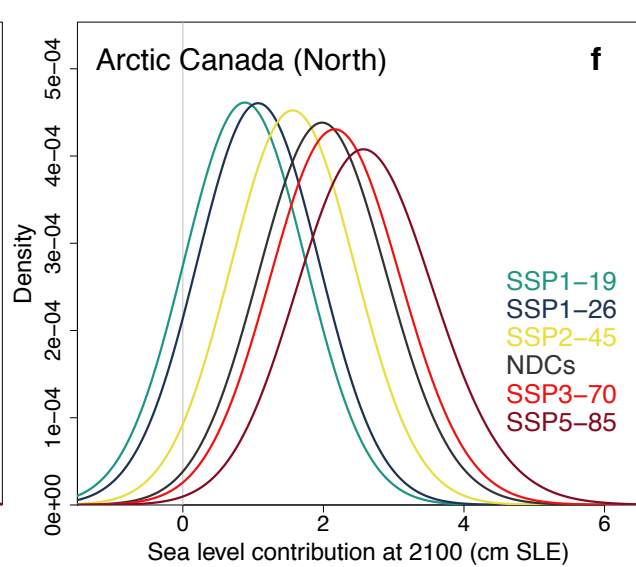
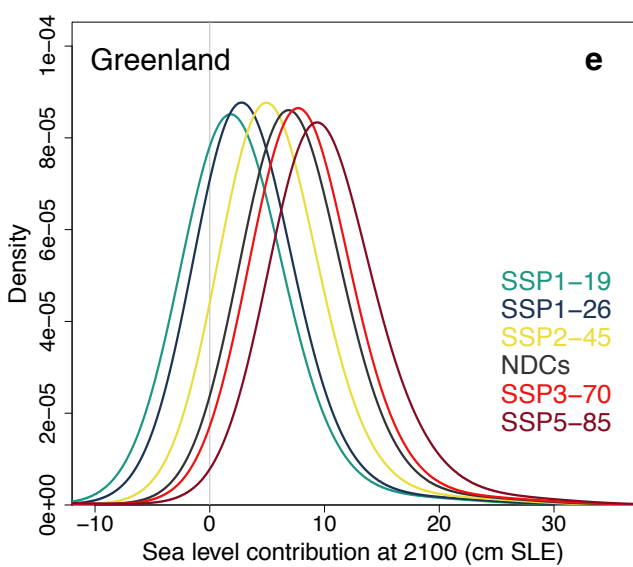
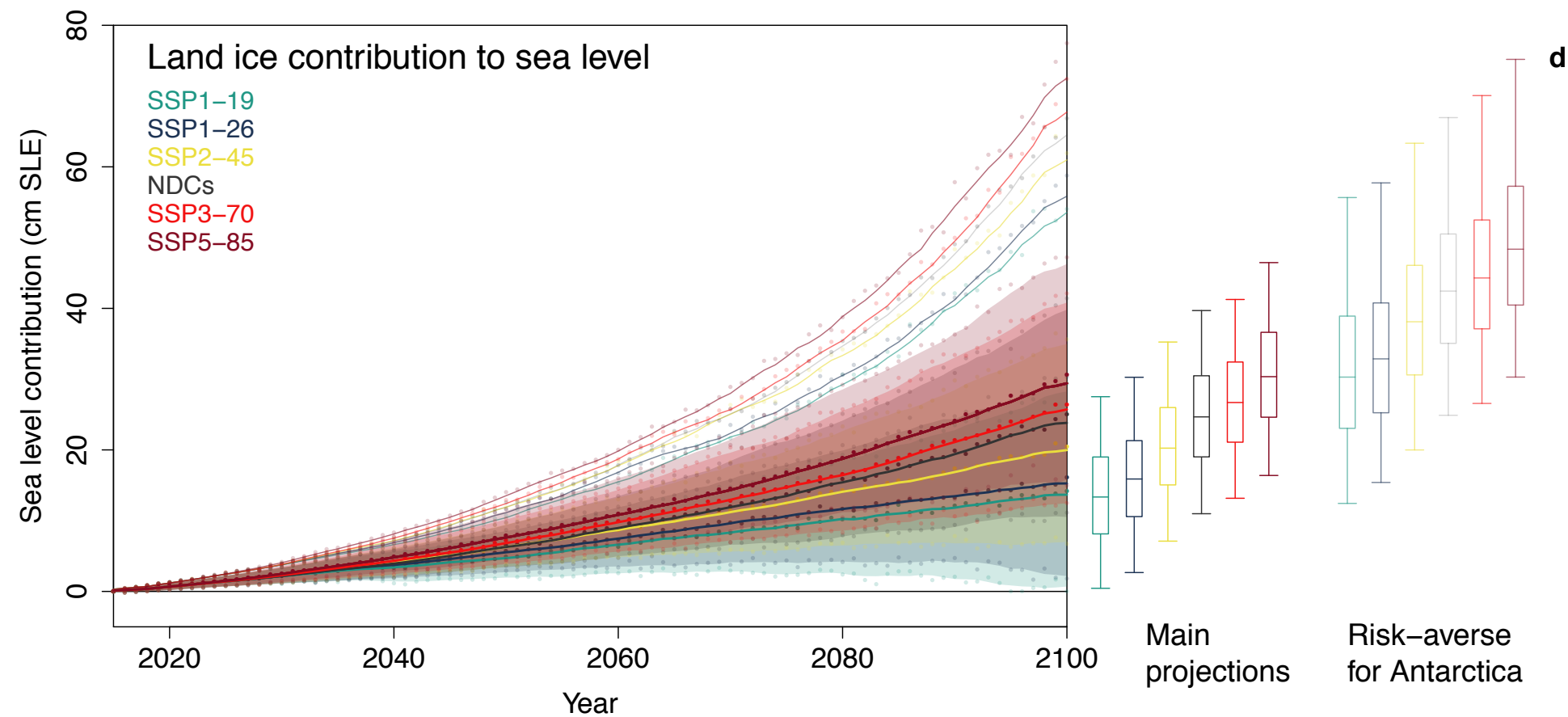
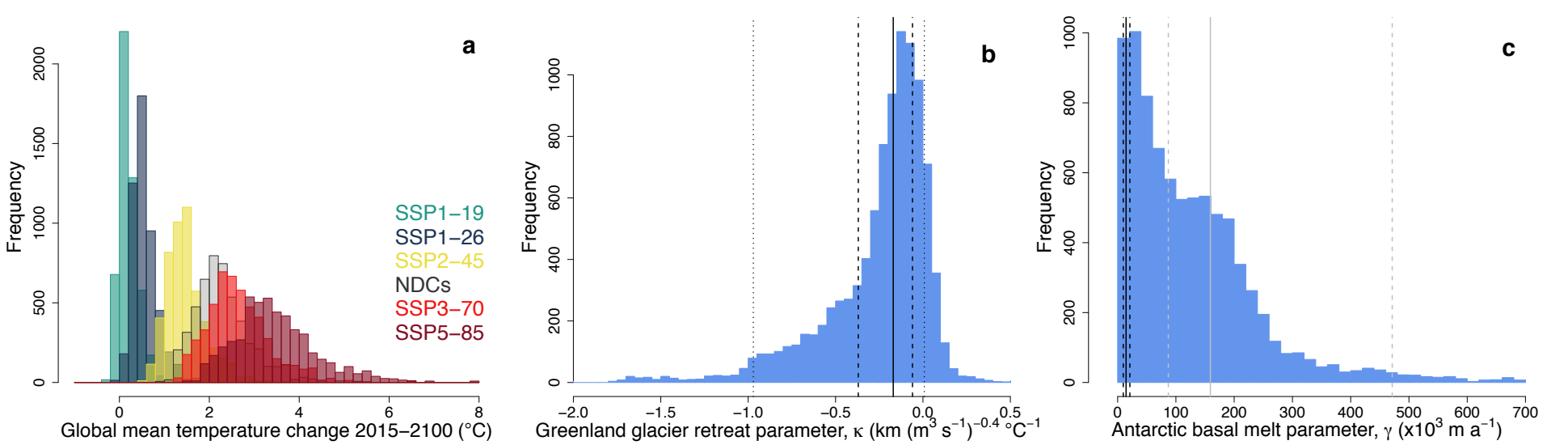
684 **Figure 4. Climate and ice sheet projections show a wide range of responses to greenhouse gas**
685 **emissions scenario.** Sea level contribution at 2100 under high greenhouse gas emissions scenarios
686 (RCP8.5 or SSP5-85) versus low scenarios (RCP2.6 or SSP1-26), categorised by climate model
687 forcing (NorESM1-M and IPSL-CM5A-MR use RCPs; CNRM-CM6-1 use SSPs), without ice shelf
688 collapse. a, Greenland. b, West Antarctica. c, East Antarctica. d, Antarctic Peninsula. Filled circles
689 show ice sheet models that use the ISMIP6 parameterisations of the ice-ocean interface, while open
690 circles show models that used their own. Simulations in the red shaded regions have more mass loss
691 under high emissions (RCP8.5/SSP5-85) than low (RCP1-26/SSP1-26); those in the green shaded
692 regions have more mass gain under high emissions scenarios than low. Two regions with other
693 possible combinations are also labelled.

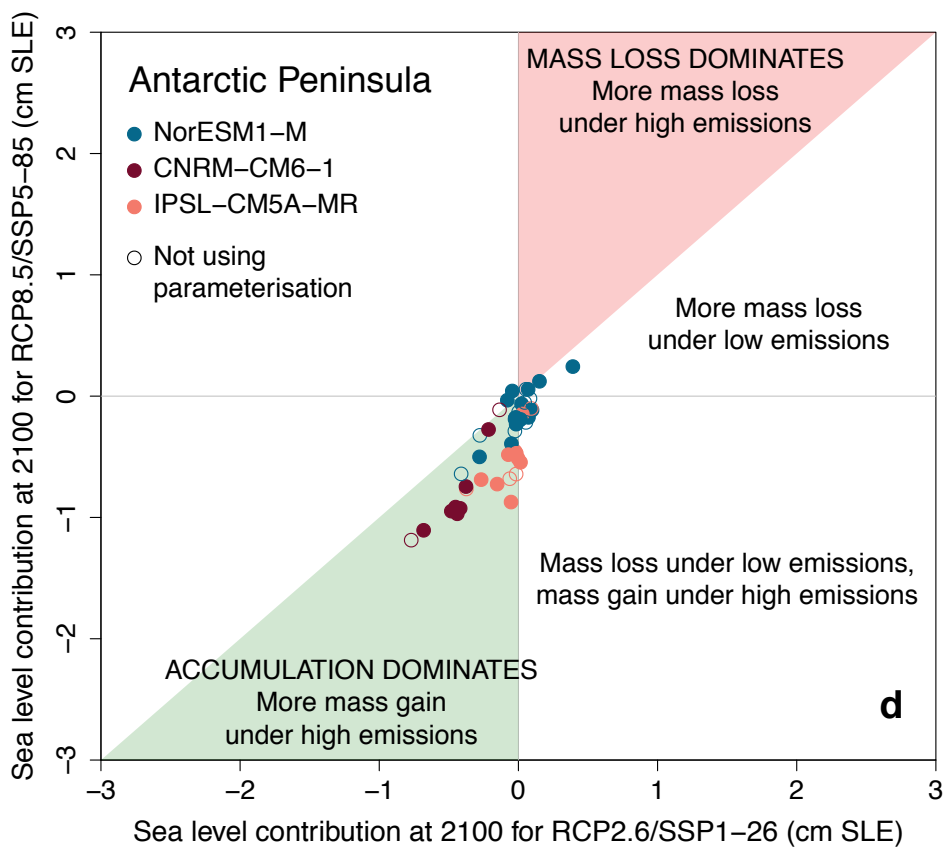
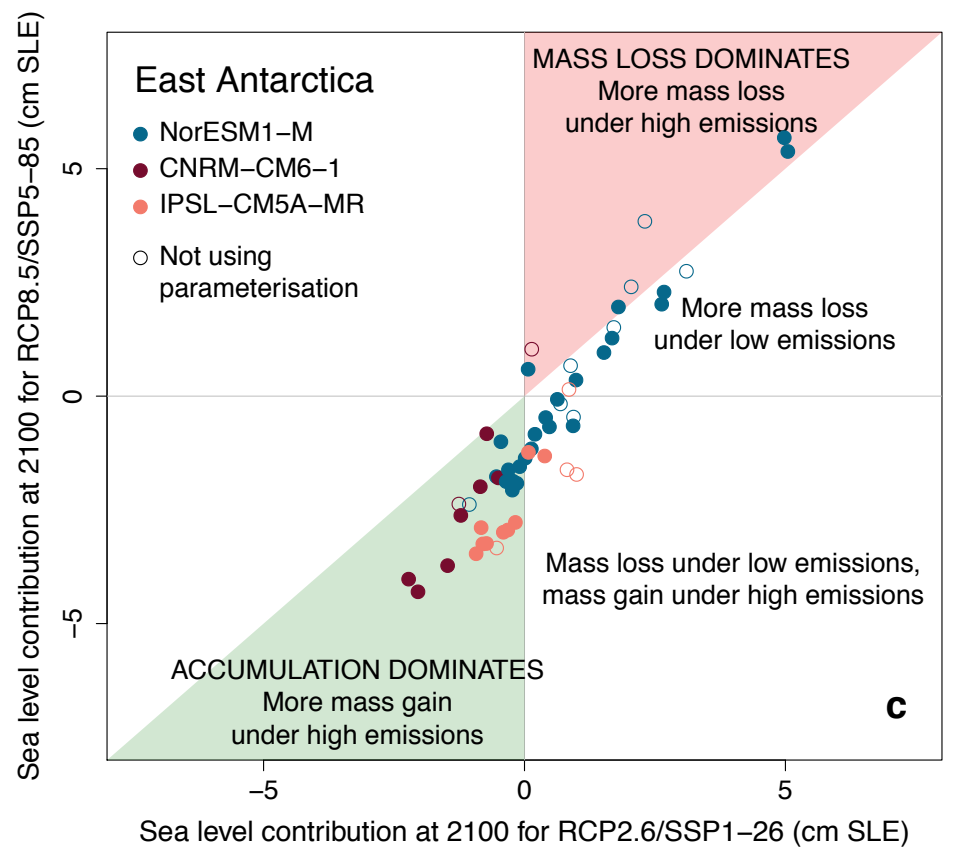
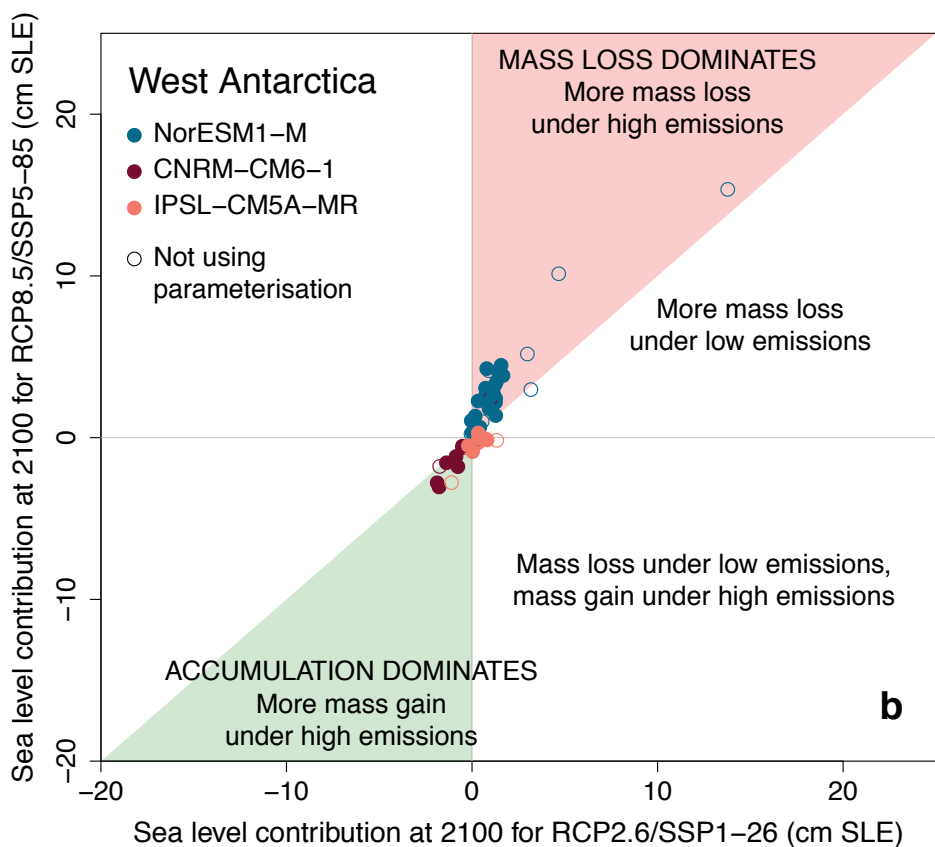
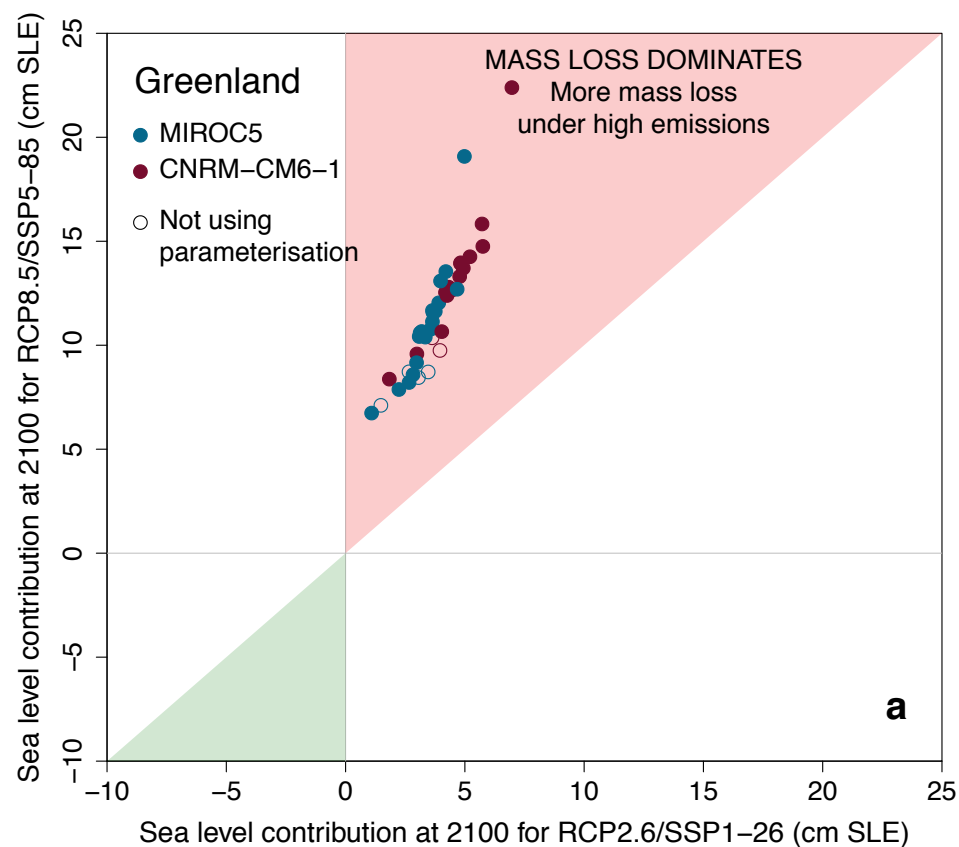
694
695 **Table 1. Projected land ice contributions to sea level rise in 2100 under different greenhouse gas**
696 **scenarios and Antarctic modelling assumptions.** Projected changes to global glaciers, Greenland
697 and Antarctic ice sheets and land ice total from 2015-2100 in sea level equivalent (cm SLE) for five
698 Shared Socioeconomic Pathways (SSPs) and predicted emissions under the 2019 Nationally
699 Determined Contributions (NDCs). Ice sheet projections do not include pre-2015 response, which is
700 estimated to add less than 1 cm to the Greenland contribution and ~2 cm to the Antarctic (see
701 Methods). The glaciers include the Greenland and Antarctic ice sheet peripheral glaciers; the overlap
702 of Antarctic periphery glaciers with the ice sheet contribution is estimated to be less than 1 cm SLE.

703
704
705
706
707
708
709









710 **Methods**

711 **Simulations**

712

713 *Ice sheet and glacier model simulations*

714

715 Ice sheet and glacier simulations are from the Ice Sheet Model Intercomparison Project 6
716 (ISMIP6)^{2,3} and Glacier Model Intercomparison Project Phase 2⁸. Most are published
717 elsewhere^{8,14-16}. Additional simulations were run for this analysis (Extended Data Table 1) as
718 follows, where the names are group/model: 22 new Greenland experiments using [5th, 95th]
719 percentile values of the retreat parameter under different climate model forcings with
720 IMAU/IMAUICE1, and 113 Antarctic experiments with CPOM/BISICLES (N = 16),
721 ILTS_PIK/SICOPOLIS (N = 31), JPL1/ISSM (N = 10), LSCE/GRISLI (N = 30) and
722 NCAR/CISM (N = 26). Eight of the new Antarctic simulations were previous experiments
723 described in ref. [15] using a new model (CPOM/BISICLES), and the rest (105) used 37 new
724 combinations of previous uncertainties for additional exploration of basal melt (29) and ice
725 shelf collapse (5) under different climate model forcings, and the interaction of ice shelf
726 collapse and basal melt (3). CPOM/BISICLES is described in the ISMIP6 Antarctic
727 initialisation study⁷: here the B variant is used, but with minimum resolution 1 km rather than
728 0.5 km. All ice sheet projections are calculated relative to a control simulation with constant
729 present day climate (see 'Comparison with IPCC assessments' for an estimate of the
730 'committed' contribution this removes).

731

732 The glacier regions are listed in Extended Data Table 2 and all simulations are described in
733 ref [8]. Greenland ice sheet projections have the peripheral glaciers (region 5) masked out, so
734 there is no double-counting. The Antarctic periphery glaciers (region 19) are located only on
735 the surrounding islands, not on the mainland ice sheet; ice sheet models include some of the
736 larger islands, so there is some overlap in area, but the effect of this is estimated to be small
737 (see 'Comparison with IPCC assessments' for an estimate of this and other limitations).

738

739 All projections are calculated as annual global mean sea level contributions since 2015,
740 converting mass (for the glaciers) or mass above flotation (for the ice sheets) to sea level
741 contribution using 362.5 Gt per mm SLE.

742

743

744 *Global climate model simulations*

745

746 We use projections of annual global mean surface air temperature change since 2015 from
747 the CMIP5 and CMIP6 global climate models used to drive the ice sheet and glacier models
748 to build the emulator. If multiple realisations (different initial conditions) for a model were
749 available, we use the mean of these. Data from 1850-2100 were downloaded from the
750 JASMIN/CEDA archive and ESGF on the 7th November 2019 and and 4th December 2019;
751 the CMIP6 snapshot was updated 28th-29th July 2020.

752

753 **Emulation**

754

755 An emulator is a fast statistical approximation of a computationally expensive simulator. This
756 can be used to predict the simulator response at untried input values – to explore the
757 uncertain input space far more thoroughly – for sensitivity analysis, to adjust the chosen
758 inputs, and to estimate probability distributions. We construct statistical models of the
759 simulated ice sheet and glacier sea level contribution as a function of the global mean surface
760 air temperature of the driving climate models – and also different representations of the ice
761 sheet-ocean interface – to make predictions under new emissions scenarios that incorporate
762 these uncertainties, as well as those arising from the different structures of the climate and ice
763 sheet models (and the emulators themselves).

764

765 Typically emulation is performed for one model at a time²⁴, but here we emulate each multi-
766 model ensemble all at once. This is made possible by the systematic design of the ISMIP6
767 and GlacierMIP projects, which explore uncertainties in global climate change and three ice-
768 ocean parameters simultaneously, and by our approach of applying emulation to multiple
769 models rather than (as is usual) one. The three ice-ocean parameters control: (1) how much
770 Greenland marine-terminating glaciers retreat (κ) with increasing local ocean temperatures
771 and meltwater runoff; (2) how much Antarctic ice-shelf basal melting (γ) increases with
772 increasing local ocean temperature; and (3) an on/off scenario of Antarctic ice shelf collapse
773 (C), which can increase glacier flow into the ocean when atmospheric temperatures rise⁴⁶.

774

775 We predict the 23 land ice regions separately – the Greenland ice sheet, the West and East
776 Antarctic ice sheets and Antarctic Peninsula, and 19 glacier regions – so the spatial
777 distribution of meltwater can be used in regional sea level projections.

778

779 We choose and evaluate emulator structures using the year 2100 (Extended Data Table 2;
780 Extended Data Figures 1 and 2). Global mean surface air temperature projections are taken
781 from the FaIR simple climate model³⁰, because it can explore uncertainties more thoroughly
782 than the relatively small CMIP6 ensemble of (computationally expensive) general circulation
783 models. We use the same global mean temperature value across all land ice sources for each
784 individual estimate: in other words, we include any co-dependence arising from global
785 temperature. Full details are described in the following sections.

786

787 *Global mean surface air temperature*

788

789 Previous sea level emulation studies^{25,26,28,29} have typically used global mean temperature as
790 the main input, rather than regional climate variables. We follow this approach for several
791 reasons: to include correlation of land ice regions induced by global climate change (i.e. no
792 need to assume/estimate their correlations, or to treat them as independent), and to have a
793 larger sample of climate change projections. Using regional climate variables would improve
794 the signal to noise for the emulator, but would restrict us to using computationally expensive
795 general circulation models from CMIP5/6, for which there only a few tens of models. The
796 simple climate model FaIR can be used to explore uncertainties in each scenario thoroughly,
797 using the latest assessments of equilibrium climate sensitivity.

798

799 Global mean temperature is the only regressor for the glacier regions. For the ice sheets, there
800 are additional terms derived from the ISMIP6 parameterisations of ice-ocean interactions.

801

802 *Ice sheet model parameters*

803

804 The Greenland glacier retreat parameter κ (Fig. 3a; units $\text{km} (\text{m}^3 \text{s}^{-1})^{-0.4} \text{°C}^{-1}$) is a scaling
805 coefficient relating marine-terminating glacier retreat to ocean temperatures and meltwater
806 runoff^{10,11}, where larger negative values indicate greater retreat of the glacier terminus in
807 response to warming. This is a continuous variable, but most simulations use one of three
808 values: the default, which is the median of the distribution in the parameterisation¹¹, $\kappa_{50} =$
809 -0.17 , and the quartiles $\kappa_{25} = -0.37$ and $\kappa_{75} = -0.06$. One model uses 5th and 95th percentile
810 values, $\kappa_5 = -0.9705$ and $\kappa_{95} = 0.0079$. For ice sheet models that did not use this
811 parameterisation ($N = 29$ simulations)¹⁴, we assign the mean value from the other simulations

812 to minimise the impact on the emulator ($\kappa = -0.2073$). One of these models (BISICLES) also
813 ran 'high' and 'low' retreat experiments by doubling and halving the ocean thermal forcing, to
814 which we assign the κ_{25} and κ_{75} values.

815

816 The Antarctic sub-shelf basal melt parameter γ (Fig. 3b; units m a^{-1}) is the 'ocean heat
817 exchange velocity' scaling coefficient relating sub-shelf basal melting to ocean
818 temperatures^{12,13}. Two alternative distributions for γ were derived in the parameterisation¹³:
819 the first from mean Antarctic melt rates, and the second from the 10 highest observations of
820 melt rate at the grounding line of Pine Island Glacier, where melt rates are currently highest.
821 The values of γ estimated from Pine Island Glacier are an order of magnitude larger, and the
822 two distributions do not overlap. This is a continuous variable, but most simulations use one
823 of three values: the default, which is the median of the Mean Antarctic distribution,
824 $\text{MeanAnt}_{50} = 14477$, and the 5th and 95th percentiles, $\text{MeanAnt}_5 = 9619$ and $\text{MeanAnt}_{95} =$
825 21005 . Further simulations used the same percentiles from the Pine Island Glacier
826 distribution: $\text{PIG}_{50} = 159188$, $\text{PIG}_5 = 86984$ and $\text{PIG}_{95} = 471264$. Some models¹⁵ used an
827 alternative variant of the parameterisation in which only local ocean temperatures were used,
828 rather than a combination of local and regional, which uses a different tuning for γ . However,
829 the values used are also the 50 [5, 95]th percentiles of those distributions, so we consider them
830 equivalent. For ice sheet models that did not use this parameterisation ($N = 62$ simulations),
831 we again assign the ensemble mean value ($\gamma = 59317$).

832

833 The Antarctic ice shelf collapse parameter C is a switch that indicates whether a scenario of
834 ice shelf collapse was used, which can lead to glacier speed-up. A timeline of collapses was
835 derived according to the presence of surface meltwater on ice shelves above a threshold (725
836 mm a^{-1}) for 10 years, estimated from surface air temperature projections⁴⁶ in the global
837 climate model driving the ice sheet model (mostly CCSM4). This method does not predict
838 whether meltwater may be efficiently drained from the surface for a given ice shelf⁴⁷, thus
839 avoiding collapse. We use values of 1 or 0 indicating whether the scenario is implemented or
840 not.

841

842 *Gaussian Process emulation*

843

844 Gaussian Process emulation⁴⁸ is non-parametric, treating the simulator as an unknown
845 mathematical function of its inputs. We use the R package RobustGaSP⁴⁹ for its numerically

846 robust parameter estimation⁵⁰. There are 23 emulators for the 2100 projections (Greenland ice
847 sheet, three Antarctic ice sheet regions, and 19 glacier regions) and 1955 emulators for the
848 full land ice time series (23 regions for each year from 2016 to 2100). An alternative to
849 predicting each year separately would be to model the temporal correlation explicitly, but we
850 prefer to use the simpler method, with fewer judgments, and allow temporal correlation to
851 emerge.

852

853 *Nugget*

854

855 We use a 'nugget' term to incorporate simulations from each multi-model ensemble. The
856 nugget is usually zero for deterministic models – the emulator predicts each simulation in the
857 ensemble exactly, i.e. the regression curve goes through all points – or a very small value, to
858 improve numerical stability or other properties^{22,23}. Here we allow the emulator to estimate
859 the nugget, and treat each multi-model ensemble as a set of outputs from a single stochastic
860 simulator or set of noisy observations. This approach has previously been used for emulating
861 stochastic simulators⁵¹ and for emulating climate models accounting for internal variability,
862 other inert inputs (uncertainties not explicitly modelled in the emulator), and approximations
863 of the model outputs⁵²⁻⁵⁷. Our method is similar to the use of 'emergent constraints' for
864 climate models^{44,58}, seeking relationships between past and future simulations across multi-
865 model ensembles to constrain them with observations, but here the predictors are inputs to the
866 models rather than their outputs for the past.

867

868 This approach does not require the simulations to be normally distributed but does assume
869 they are independent, which has been a long-standing difficulty of interpreting multi-model
870 climate ensembles. But with ice sheet models, although model names may be the same across
871 groups, each one has a very different set up, including physics approximations,
872 parameterisations, tuning, grid resolution, and – in particular – initialisation methods, which
873 have been shown to produce very different results even for simulations produced by the same
874 group^{6,7,14,15,59-61}. For glacier models, their structures are also vastly different, ranging from
875 simple scaling parameterisations to dynamic physical models⁸. We test two approaches to
876 account for any model dependence: a dummy variable (see below) and random effects
877 ('Antarctic cross-check model').

878

879 *Statistical model*

880

881 Let y denote the simulated global mean sea level contribution for given region and year (in
882 cm SLE), and \mathbf{x} the simulator inputs (see below). Following ref. [22], we write the simulator
883 as a function $y = f(\mathbf{x})$, for which the Gaussian Process emulator is described by a mean
884 function:

$$885 \quad E[f(\mathbf{x})] = \mathbf{h}(\mathbf{x})^T \boldsymbol{\beta},$$

886

887 where $\mathbf{h}(\mathbf{x})$ is a vector of regression functions and $\boldsymbol{\beta}$ the corresponding regression coefficients,
888 and a covariance function, with variance σ^2 and correlation function $c(\mathbf{x}, \mathbf{x}')$,

889

$$890 \quad \text{Cov}[f(\mathbf{x}), f(\mathbf{x}')] = \sigma^2(c(\mathbf{x}, \mathbf{x}') + \nu \mathbf{I}),$$

891

892 where ν is the nugget term and \mathbf{I} the identity matrix. So the prior for $f(\mathbf{x})$ is:

893

$$894 \quad p(f(\mathbf{x}) \mid \boldsymbol{\beta}, \sigma^2, \delta, \nu) \sim N(\mathbf{h}(\mathbf{x})^T \boldsymbol{\beta}, \sigma^2(c(\mathbf{x}, \mathbf{x}') + \nu \mathbf{I})),$$

895

896 where \mathbf{x} are whichever model inputs are used for a given region, δ are the correlation lengths
897 of the covariance function, and $\sigma^2\nu$ is the variability not explained by the inputs. Parameters
898 ($\boldsymbol{\beta}, \sigma^2, \delta, \nu$) are estimated from the simulation data.

899

900 The inputs \mathbf{x} used in the regression functions are global mean temperature change, T , and, for
901 the ice sheets, the ice-ocean parameter values (κ for Greenland; γ, C for Antarctica), plus a
902 dummy variable denoting whether Greenland models used the retreat parameterisation. These
903 are discussed in the next section. All inputs are rescaled to have zero mean and unit variance.

904

905 *Mean functions*

906

907 The Gaussian Process mean function describes the large-scale response of the simulator to its
908 inputs, usually specified as a linear trend with the remainder described by a zero-mean
909 Gaussian process.

910

911 For the glaciers, the linear regressor is simply global mean temperature in the same year (T).

912 For the ice sheets, the additional ice sheet model parameters are κ for Greenland, and γ and C

913 for Antarctica. We also try two types of dummy variable. The first is for the ice sheet and
 914 glacier model names, so these can be treated distinctly in the emulator, but this leads to clear
 915 overfitting (i.e. the model is too flexible in Figs. 1 and 2). The second represents whether an
 916 ice sheet model uses the ISMIP6 retreat or basal melt parameterisation, to absorb any
 917 misalignment between the imputed value and the effective value. Bayesian Information
 918 Criterion (BIC) from a stepwise model selection (testing up to first-order interactions)
 919 suggests this dummy variable is informative for Greenland, so we retain it (o , for open
 920 parameterisation), but not for the Antarctic regions. The stepwise model selection suggests
 921 we could reasonably include terms for the interaction between temperature and retreat for
 922 Greenland, temperature and basal melt for West Antarctica, and temperature and collapse for
 923 East Antarctica, but we choose not to, to avoid the risk of overfitting. The selection also
 924 shows that collapse strongly dominates the Antarctic Peninsula response, and is may not be
 925 needed for West Antarctica, but we retain all terms (i.e. T_i, γ_0, C) because we otherwise find
 926 the covariance matrix is poorly conditioned. The resulting mean functions are $h_{\text{GIS}}(\mathbf{x})_i \sim (T_i,$
 927 $k, o)$ for Greenland, $h_{\text{AIS}}(\mathbf{x})_i \sim (T_i, \gamma_0, C)$ for the Antarctic regions, and $h_{\text{Glaciers}}(\mathbf{x})_i \sim (T_i)$ for the
 928 glaciers, where $h \sim (a, b)$ means h is a linear function of a and b , and i is the index for the
 929 year.

930

931 *Covariance functions*

932

933 The covariance function describes the smoothness of the Gaussian Process. As in any
 934 statistical modelling, there is a trade-off between improving accuracy and over-fitting. We
 935 assess this using the usual leave-one-out procedure^{62,63}. We fit the emulator to all ensemble
 936 members but one, then predict the sea level contribution from this simulation; we repeat this
 937 for every combination, noting the emulator error (residual) and uncertainty for each
 938 prediction. We perform this for each of the 23 regional emulators for the year 2100 with five
 939 covariance functions of varying smoothness – Matérn(5/2), which is the default in
 940 RobustGaSP, Matérn (3/2), and three members of the power exponential family with high,
 941 medium and low exponent values ($\alpha = 1.9$, i.e. close to a squared exponential, the default
 942 value; $\alpha = 1.0$, exponential, and $\alpha = 0.1$, for which the covariance function has a small effect
 943 so the emulator approaches linear regression).

944

945 For 18 of the 19 glacier regions, we use the covariance function with the smallest
 946 standardised Euclidean distance between the emulator predictions and simulations

947 (standardised because, unlike simpler metrics such as root mean square error or mean
948 absolute error, it does not penalise larger errors if the emulator uncertainty intervals are
949 sufficiently large), as in ref [24]. For the Southern Andes (region 17), all covariance functions
950 give identical distances, so we use the default for RobustGaSP. For the ice sheets, we use the
951 covariance function that gives close to linear regression (power exponential, $\alpha = 0.1$), rather
952 than the one with the minimum Euclidean distance, for various reasons. For Greenland, West
953 Antarctica, and the Antarctic Peninsula, the minimum distance covariance functions (power
954 exponential $\alpha = 1.0$ for Greenland; Matérn(3/2) for the Antarctic regions) result in overfitting
955 for temperature (i.e. too much flexibility in Fig. 1). For East Antarctica, the minimum
956 distance covariance functions (Matérn(5/2)) result in an incorrect sign prediction under the
957 ice shelf collapse switch. Using the alternative covariance function solves all of these issues
958 and does not increase the standardised Euclidean distance by much: 4% for the Peninsula,
959 and 0.4-1% for the other three regions. The resulting covariance functions are given in
960 Extended Data Table 2.

961

962 *Evaluating the emulators*

963

964 After selecting the covariance functions for each regional emulator at 2100, we evaluate the
965 emulators further by plotting the emulator predictions against the simulations from the leave-
966 one-out procedure, and the standardised residuals (the difference between the emulator
967 prediction and the simulator, divided by the emulator standard deviation), and calculating the
968 percentage of simulations falling within ± 2 s.d. (Extended Data Table 2 and Extended Data
969 Figures 1 and 2). We would not expect exactly 95% of the simulations to fall within 2 s.d., in
970 part because the predictions are not independent, but very low or high values would suggest
971 emulator over- or under-confidence. The region with the lowest percentage of predictions
972 within the uncertainty intervals is North Asia (region 10) with 89%, indicating slightly too
973 small emulator uncertainty estimates, and the highest is 98% (Scandinavia: region 8),
974 indicating the reverse.

975

976 Mean absolute errors for each emulator are given in Extended Data Table 2 and Extended
977 Data Figures 1 and 2: for the ice sheet regions they are 0.28 cm (Peninsula), 1.4 cm
978 (Greenland) and 1.5 cm (East Antarctica) and 2.0 cm (West Antarctica), and for the

979 individual glacier regions they range from 0.0020 cm to 0.87 cm (Antarctic periphery: region
980 19). Mean absolute standardised errors are all less than 0.006.

981

982 The emulator underestimates the three to four highest West and East Antarctic contributions
983 by around 10-15 cm (Extended Data Figure 1b and 1c). The five highest of these are from the
984 SICOPOLIS model, which has a much greater sensitivity to basal melting than other models
985 (see main text, *Robustness checks* and Extended Data Figure 6), and use the highest value of
986 this parameter ($\gamma = \text{PIG}_{95}$). These simulations are therefore extreme: 1% of the 344
987 simulations, and the 97.5th percentile value of the basal melt parameter. There are process-
988 based reasons to expect that SICOPOLIS is an upper bound or overestimate (see main text).
989 When the emulator is calibrated with this model alone, it does not underestimate its highest
990 contributions (not shown). The resulting projections under the NDC scenario are shown in
991 *Robustness checks* (test 4); the difference with the main projections may be interpreted as the
992 maximum possible impact of this emulator underestimate, if SICOPOLIS were the sole
993 realistic ice sheet model. These are lower than the 'risk-averse' projections, which are made
994 with a subset of high sensitivity ice sheet models and other pessimistic assumptions (see main
995 text).

996

997 We therefore consider the emulators to be adequate for the predictions of large-scale sea level
998 contribution presented here.

999

1000 *Antarctic cross-check model*

1001

1002 We perform a cross-check for the Antarctic ice sheet regions at 2100 using a linear mixed
1003 model, with the ice sheet model name included as a random effect to deal with any systematic
1004 uncertainty arising from dependence of ensemble members. This attributes some of the
1005 uncertainty in the response to the ice sheet model used, and this uncertainty can then be
1006 removed from the predicted PDF. We thus model the ensemble members as 'similar but not
1007 identical', using a mean function of temperature and ice sheet parameters, plus a structured
1008 error term which includes a systematic component according to the ice sheet model and a
1009 noise component to capture other sources of variability such as initialisation.

1010

1011 For the mean function (also linear), we use the logarithm of γ as a regressor, so it is always
1012 positive. Consequently we use the geometric mean as the missing value, rather than the
1013 arithmetic mean. We use a dummy variable to denote these models, as for Greenland in the
1014 GP emulator. The full global mean temperature change trajectories are used instead of only
1015 the total change at 2100. To increase the signal-to-noise ratio, the annual means are reduced
1016 to decadal means (2015–2029, 2030–2039, . . . , 2090–2100). There are thirteen distinct
1017 forcings, each one the product of a global climate model and a scenario, so we represent the
1018 forcing variables as twelve bisquare basis functions. These start as thirteen bisquare basis
1019 functions, each one centred at one of the thirteen forcings, but one is dropped because
1020 otherwise the model matrix becomes rank deficient when a constant is added. The one
1021 dropped is the one with the smallest mean Euclidean distance to the other twelve. We use
1022 bisquare kernels, where the standard deviation of each kernel is set to one tenth of the
1023 maximum Euclidean distance between all pairs of forcings, to cover the forcing space with
1024 non-zero values for the forcing regressors. We use the same distributions for temperature,
1025 basal melt and collapse as the main projections, and set the dummy variable to represent
1026 standard parameterisation models.

1027

1028 This emulator predicts 50 [5, 95]th percentiles for the West Antarctic sea level contribution at
1029 2100 of 2 [-4, 8] cm SLE for SSP1-26 and 3 [-4, 10] cm SLE for SSP5-85, which are very
1030 similar to the GP emulator predictions of 2 [-5, 10] cm SLE and 3 [-4, 11] cm SLE. We test
1031 the effect of changing the kernel standard deviation to one twelfth or one fourteenth of the
1032 maximum Euclidean distance; the largest change is a 2 cm decrease in the 95th percentile
1033 under SSP5-85. For East Antarctica, the emulator with random effects predicts 2 [-3, 6] cm
1034 SLE for both scenarios; the GP emulator predicts a small scenario-dependence, 2 [-4, 7] cm
1035 SLE for the low emissions scenario and 0 [-5, 6] cm SLE for the high. For the Antarctic
1036 Peninsula, the random effects predictions are 0 [-1, 2] cm SLE for both scenarios, and the GP
1037 are the same. These similarities give us confidence that model dependence is not substantially
1038 affecting our projections – i.e. that differences in model structure, resolution, calibration and
1039 initialisation dominate over the similarities – although it would be worth investigating this in
1040 more detail.

1041

1042 **Sea level projections**

1043

1044 We use probability distributions for global temperature and the ice sheet model parameters as
1045 inputs to each emulator to make the projections.

1046

1047 *Global mean temperature projections*

1048

1049 We use projections of global annual mean surface air temperature change since 2015 from
1050 the FaIR (Finite amplitude Impulse Response) simple climate model for the main projections.

1051 We take the 500-member ensemble from reference [30]: SSP1-19, SSP1-26, SSP3-70, SSP5-

1052 85 and a scenario estimated for the 2019 Nationally Determined Contributions. We also use

1053 projections for SSP-245 generated with the same ensemble.

1054

1055 *Ice sheet model parameter distributions*

1056

1057 For Greenland, we sample from a kernel density estimate of the original k distribution ($N =$
1058 191) with the same bandwidth used in deriving the parameterisation^{10,11} (0.0703652) (Fig. 1b).

1059 The dummy variable is always set to represent the standard ISMIP6 parameterisation.

1060

1061 For Antarctica, we combine the Mean Antarctic and Pine Island Glacier γ distributions ($N =$
1062 10,000 each), and sample from a kernel density estimate using three times the automatic
1063 bandwidth (Silverman's 'rule of thumb'⁶⁴) to merge and smooth them into a near-unimodal
1064 distribution that we truncate at zero (Fig. 1c). For the collapse switch C , we sample randomly
1065 from 0 or 1 with equal probability (8% of the ISMIP6 simulations have ice shelf collapse).

1066 The ice shelf collapse scenario does not include the possibility of surface meltwater draining
1067 efficiently from some ice shelves under certain conditions, thereby avoiding collapse, so we
1068 feel this is a reasonable judgement.

1069

1070 *Sampling*

1071

1072 For the 2100 projections, we sample from the FaIR ensemble ($N=500$) with replacement ($N =$
1073 5000 for main and risk-averse projections; $N = 1000$ for robustness and sensitivity tests). For

1074 the full time series, we use the 500 FaIR projections directly without resampling. We make

1075 one set of emulator predictions (23 regions) for each temperature value in a given year,

1076 randomly sampling the relevant ice-ocean parameters (k , γ_0 , C) once for each FaIR ensemble

1077 member.

1078
1079
1080
1081
1082
1083
1084
1085
1086
1087
1088
1089
1090
1091
1092
1093
1094
1095
1096
1097
1098
1099
1100
1101
1102
1103
1104
1105
1106
1107
1108
1109
1110
1111

We integrate over the uncertain inputs (temperature in a given year, and ice-ocean parameters) to obtain the final probability density functions (PDFs). Each regional emulator predicts a Student-t distribution for a given set of these input values, defined by a mean and standard deviation; we approximate this with a normal distribution, as in refs [55, 57], which is accurate enough for this application. We use different integration methods for the 23 individual regional PDFs compared with the regional sums (Antarctica, global glaciers, and land ice total). For the individual regional estimates, we use deterministic numerical integration (the midpoint rule: we sum the Gaussian distributions for each emulator prediction, then normalise). For regional sums we must use Monte Carlo sampling, because the three ice sources (Greenland, Antarctica and glaciers) have different parameters, and we also desire traceability of predictions to input values within a given ice source. We sample once from the Gaussian distribution for each emulator prediction, then sum the regional samples for a given temperature to estimate the PDF, smoothing with kernel density estimation for figures (again using Silverman's 'rule of thumb'⁶⁴ for the bandwidth). Sampling is a more noisy method of integration than deterministic methods, so the PDFs for regional sums are less smooth than those for individual regions.

Glacier maximum cap

We apply a cap to the glacier projections using estimates of their maximum sea level contribution³¹. Glacier model projections often exceed this cap in some regions, if near or total loss is projected under high emissions, either because they report changes in total mass, not mass above flotation, or because of errors in initial mass⁸, or both. We restrict values to the maximum in the emulator mean predictions and then the PDFs (the latter exceeding the cap due to emulator uncertainty).

Time series smoothing

Interannual variability arises in the time series due to sampling the emulator uncertainty for each annual regional prediction. We apply a five year running mean in Fig. 3d to visualise the expected smoothness of sea level contributions; projections provided in the Supplementary Information are unsmoothed.

1112 **Comparison with IPCC assessments**

1113

1114 The ice sheet projections are made relative to control simulations with a constant recent
1115 climate. This control includes both the model drift and, depending on the initialisation
1116 method, any background contribution arising from forcing before 2015. This background
1117 contribution should be added to the ice sheet projections, but is difficult to quantify. Five year
1118 mean rates of sea level contribution since 1992/3 range from 0.1-0.8 mm/yr for the Greenland
1119 ice sheet⁶⁵ and 0.1-0.6 mm/yr for Antarctica⁶⁶, but they would decrease in the absence of
1120 forcing after 2014. Modelling work to quantify the background contribution from
1121 Greenland⁶⁷ suggests a contribution of 0.6 ± 0.2 cm SLE by 2100. Estimates made for this
1122 study range from 0.3-0.8 cm under a range of retreat parameter values, $\kappa_{75} - \kappa_{25}$
1123 (IMAU/IMAUICE1: 0.3-0.4 cm; CISM variant similar to NCAR/CISM: 0.4-0.8 cm). For
1124 Antarctica, the dynamic commitment has been estimated to be 2 cm SLE at 2100 for the
1125 Amunden Sea Embayment region of West Antarctica, where most mass loss is currently
1126 occurring⁶⁸. Part of these trends may still be due to residual model drift. The committed
1127 contribution could therefore add up to ~ 1 cm/century to our Greenland projections and ~ 2
1128 cm/century to the Antarctic.

1129

1130 The Antarctic ice sheet models include some of the larger islands that are also included in
1131 region 19, potentially leading to double-counting. However, median projections for region 19
1132 range from 1-2 cm under different emissions scenarios, and the ice sheet models are much
1133 lower resolution (i.e. the glaciers are likely less responsive), so the effect is expected to be of
1134 order 0.5-1 cm SLE or less.

1135

1136 We average our projections over the 86 years and compare them with the average IPCC
1137 AR5²⁵ and SROCC¹ projections over 95 years (the midpoints of 1986-2005 to 2081-2100) as
1138 rates of cm SLE per century. For the glaciers, we project 8 cm/century SLE for SSP1-26 and
1139 16 cm/century for SSP5-85 excluding the Antarctic peripheral glaciers (region 19: 1 cm and 2
1140 cm, respectively), compared with 10 cm for RCP2.6 and 17 cm for RCP8.5 in AR5. For the
1141 Greenland ice sheet, we project 4 cm/century SLE for SSP1-26 and 11 cm for SSP5-85,
1142 compared with 6 cm for RCP2.6 and 13 cm for RCP8.5 in AR5. For Antarctica, we project 5
1143 cm/century SLE for both scenarios; the AR5 projections are 5 cm/century SLE for RCP2.6
1144 and 4 cm for RCP8.5, while those for SROCC are 4 cm/century SLE for RCP2.6 and 11 cm

1145 for RCP8.5. The difference between scenarios for Antarctica in AR5 arises only from
1146 additional accumulation, because the dynamic contributions are assumed to be the same.

1147

1148 Glacier projections could be overestimated because meltwater routing to the ocean is not
1149 accounted for (not all volume lost from the glaciers reaches the oceans), or underestimated
1150 because only one glacier model includes ice-water interactions (i.e. frontal ablation of
1151 marine- and lake-terminating glaciers). For the latter, we compare mean projections for the
1152 GloGEM model to the emulator for RCP8.5/SSP5-85 and RCP4.5/SSP2-45 for key regions,
1153 and find they are larger by less than 1 cm for Alaska and Russian Arctic (regions 1 and 9), by
1154 less than 0.5 cm for Svalbard (7) and Arctic Canada South (4), and smaller than the emulator
1155 for Arctic Canada North (3). All are within the emulator 95th percentile estimates. We may
1156 slightly underestimate uncertainty in the global glacier total due to correlated errors across
1157 models⁸ by emulating the regions independently, though there are compensating advantages
1158 (more accurate emulation; spatial pattern of meltwater); a similar argument applies to
1159 Antarctica.

1160

1161 **Sensitivity tests**

1162

1163 We perform a number of checks to test the sensitivity of the ice sheet projections to changes
1164 in the chosen inputs, predominantly the input distributions, but also the dataset in the final
1165 test (see Extended Data Table 3 and refs [25, 26,30, 34, 39]). All results are shown for the
1166 SSP5-85 scenario in Extended Data Figure 4 under the index given (where 1 is the main
1167 projection); numerical values in the text refer to changes in the median and [5,95th] percentile
1168 estimates for the ice sheet under this scenario unless otherwise stated.

1169

1170 **Robustness checks**

1171

1172 We perform a number of checks to test robustness of the ice sheet projections to changes in
1173 the simulation dataset (see Extended Data Table 4 and refs [14, 16, 24, 66]). Results are
1174 shown for the NDCs scenario in Extended Data Figure 5 under the test index given (where 1
1175 is the main projection); numerical values in the text refer to changes in the median and
1176 [5,95th] percentile estimates under this scenario unless otherwise stated. The full datasets are
1177 256 simulations for Greenland and 344 simulations for Antarctica.

1178

1179 **Parameter interactions**

1180 *Retreat and basal melt vs temperature*

1181

1182 Ice sheet projection uncertainties are constant across scenarios. However, tests with three ice
1183 sheet models show that the range of projections from high to low values of the retreat
1184 parameter ($\kappa_{95} - \kappa_5$) and basal melt parameter ($PIG_{95} - \text{MeanAnt}_{50}$) is consistently smaller
1185 under RCP2.6 than RCP8.5, so the emulator uncertainty should be smaller at lower
1186 temperatures. The ratios of ranges, RCP2.6/RCP8.5, for each group/model + GCM are:

1187

1188 Greenland

1189 • IMAU/IMAUICE + MIROC5 = $1.4097/8.3069 = 0.17$

1190 • IMAU/IMAUICE + CNRM-CM6-1 = $2.4813/9.7187 = 0.26$

1191

1192 West Antarctica

1193 • JPL1/ISSM + NorESM1-M = 0.40

1194 • CPOM/BISICLES + NorESM1-M = 0.57

1195

1196 East Antarctica

1197 • JPL1/ISSM + NorESM1-M = 0.73

1198 • CPOM/BISICLES + NorESM1-M = 0.32

1199

1200 The emulator does not have sufficient data from lower emissions scenarios to reduce the
1201 variance, particularly for Greenland. If other ice sheet models respond the same way as the
1202 above, then adding more simulations may reduce the uncertainty for low SSPs.

1203

1204 *Ice shelf collapse vs basal melt*

1205

1206 The contribution due to ice shelf collapse does not increase with higher values of the basal
1207 melt parameter in the models JPL1/ISSM and CPOM/BISICLES (0.1 cm difference for the
1208 Peninsula in BISICLES; all other regional differences for both models ≤ 0.02 cm).

1209

1210

1211 **Code availability**

1212

1213 R code and input data are available at <https://github.com/tamsinedwards/emulandice>. Each
1214 simulation in the sea level projections file has a label in the 'publication' column for the
1215 reference (Goelzer2020, Seroussi2020, Nowicki2020 or Marzeion2020), or 'New' if
1216 previously unpublished.

1217

1218 **Data availability**

1219

1220 All global climate, simple climate, ice sheet and glacier model data used as inputs to this
1221 study are provided with the code as described above. Main and risk-averse projections from
1222 the analysis are provided in the Supplementary Information as annual quantiles for each of
1223 the 23 regions, and the Antarctic, glacier and land ice sums.

1224

1225 **Author information**

1226

1227 The authors declare no competing financial or non-financial interests. Correspondence and
1228 requests for materials should be addressed to T.L.E. (tamsin.edwards@kcl.ac.uk). Reprints
1229 and permissions information is available at www.nature.com/reprints.

1230

1231 **Methods References**

1232

1233 46. Trusel, L. D. *et al.* Divergent trajectories of Antarctic surface melt under two twenty-
1234 first-century climate scenarios. *Nature Geoscience* 8, 927–932 (2015).

1235 47. Bell, R. E. *et al.* Antarctic ice shelf potentially stabilized by export of meltwater in
1236 surface river. *Nature* **544**, 344–348 (2017).

1237 48. O'Hagan, A. Bayesian analysis of computer code outputs: A tutorial. *Reliability*
1238 *Engineering and System Safety* **91**, 1290–1300 (2006).

1239 49. Gu, M. *et al.*, RobustGaSP: Robust Gaussian Stochastic Process Emulation in R,
1240 *The R Journal* (2019) 11:1, pages 112–136.

1241 50. Gu, M., X. Wang and J.O. Berger (2018), Robust Gaussian stochastic process
1242 emulation, *Annals of Statistics*, 46(6A), 3038–3066.

1243 51. van Beers, W. C. M. & Kleijnen, J. P. C. Kriging for interpolation in random
1244 simulation. *Journal of the Operational Research Society* 54, 255–262 (2017).

1245 52. Salter, J. M. & Williamson, D. A comparison of statistical emulation methodologies
1246 for multi-wave calibration of environmental models. *Environmetrics* 27, 507–523
1247 (2016).

1248 53. Williamson, D. & Blaker, A. T. Evolving Bayesian Emulators for Structured Chaotic
1249 Time Series, with Application to Large Climate Models. *SIAM/ASA J. Uncertainty*
1250 *Quantification* 2, 1–28 (2014).

1251 54. Williamson, D., Blaker, A., Hampton, C. & Salter, J. Identifying and removing
1252 structural biases in climate models with history matching. *Climate Dynamics* **45**,
1253 1299–1324 (2014).

1254 55. Araya-Melo, P. A., Crucifix, M. & Bounceur, N. Global sensitivity analysis of the
1255 Indian monsoon during the Pleistocene. *Climate of the Past* **11**, 45–61 (2015).

1256 56. Bounceur, N., Crucifix, M. & Wilkinson, R. D. Global sensitivity analysis of the
1257 climate–vegetation system to astronomical forcing: an emulator-based approach.
1258 *Earth Syst. Dynam.* **6**, 205–224 (2015).

1259 57. Lord, N. S. *et al.* Emulation of long-term changes in global climate: application to
1260 the late Pliocene and future. *Climate of the Past* **13**, 1539–1571 (2017).

1261 58. Bowman, K. W. *et al.* (2018). A hierarchical statistical framework for emergent
1262 constraints: Application to snow-albedo feedback. *Geophysical Research Letters*, 45,
1263 13,050–13,059. <https://doi.org/10.1029/2018GL080082>

1264 59. Nowicki, S. *et al.* Insights into spatial sensitivities of ice mass response to
1265 environmental change from the SeaRISE ice sheet modeling project I: Antarctica. *J*
1266 *Geophys Res-Earth* **118**, 1002–1024 (2013).

1267 60. Nowicki, S. *et al.* Insights into spatial sensitivities of ice mass response to
1268 environmental change from the SeaRISE ice sheet modeling project II: Greenland. *J*
1269 *Geophys Res-Earth* **118**, 1025–1044 (2013).

1270 61. Saito, F., Abe-Ouchi, A., Takahashi, K. & Blatter, H. SeaRISE experiments revisited:
1271 potential sources of spread in multi-model projections of the Greenland ice sheet. *The*
1272 *Cryosphere* **10**, 43–63 (2016).

1273 62. Rougier, J., Sexton, D. M. H., Murphy, J. M. & Stainforth, D. A. Analyzing the
1274 Climate Sensitivity of the HadSM3 Climate Model Using Ensembles from Different
1275 but Related Experiments. *J Climate* **22**, 3540–3557 (2009).

1276 63. Bastos, L. S. & O'Hagan, A. Diagnostics for Gaussian Process Emulators.
1277 *Technometrics* **51**, 425–438 (2009).

1278 64. Silverman, B. W. (1986). *Density Estimation*. London: Chapman and Hall.

- 1279 65. The IMBIE team. Mass balance of the Greenland Ice Sheet from 1992 to 2018. *Nature*
1280 1–25 (2019). doi:10.1038/s41586-019-1855-2
- 1281 66. The IMBIE team. Mass balance of the Antarctic Ice Sheet from 1992 to 2017. *Nature*
1282 **558**, 219–222 (2018).
- 1283 67. Price, S. F., Payne, A. J., Howat, I. M., and Smith, B. E.: Committed sea-level rise for
1284 the next century from Greenland ice sheet dynamics during the past decade, *P. Natl.*
1285 *Acad. Sci. USA*, 108, 8978–8983, 2011.
- 1286 68. Alevropoulos-Borrill, A. V., Nias, I. J., Payne, A. J., Golledge, N. R. & Bingham, R.
1287 J. Ocean-forced evolution of the Amundsen Sea catchment, West Antarctica, by 2100.
1288 *The Cryosphere* **14**, 1245–1258 (2020).
1289
1290

1291 **Extended Data**

1292

1293 **Extended Data Table 1. The additional 22 Greenland and 37 Antarctic ice sheet model experiments**

1294 **not previously described elsewhere.** Retreat parameter values κ_5 and κ_{95} are the 5th and 95th percentile
1295 values of the retreat (κ) distribution; basal melt parameter values $\text{MeanAnt}_{[5, 50, 95]}$ and $\text{PIG}_{[5, 50, 95]}$ are the
1296 5th, 50th and 95th percentile values of the Mean Antarctic and Pine Island Glacier basal melt (γ)
1297 distributions (see Methods).

1298

1299 **Extended Data Table 2. Emulator structure and validation.** Emulator covariance functions, and the
1300 results of the leave-one-out procedure for each: the percentage of simulations that fall within the emulator
1301 95% uncertainty intervals, and the mean absolute error.

1302

1303 **Extended Data Figure 1. Emulator leave-one-out validation for ice sheets and 8 glacier regions.** Left

1304 of each subpanel: Emulator predictions versus simulations for each regional sea level contribution in the
1305 year 2100, with percentage of predictions falling outside ± 2 emulator standard deviations and mean
1306 absolute error in cm SLE. Right of each subpanel: standardised residuals (emulated minus simulated,
1307 divided by emulator standard deviation). Predictions falling outside ± 2 emulator standard deviations are
1308 shown in orange.

1309

1310 **Extended Data Figure 2. Emulator leave-one-out validation for 11 glacier regions.** As for Extended
1311 Data Figure 1, but for the remaining glacier emulators.

1312

1313 **Extended Data Figure 3. Temperature projections for 2015-2100 from FaIR and CMIP6 ensembles.**

1314 Global surface air temperature projections under different greenhouse gas scenarios (see main text) from
1315 the (a) FaIR simple climate model ensemble ($N = 5000$; same as Figure 3a) and (b) CMIP6 global climate
1316 model ensemble ($N \sim 30$ models per scenario: see Methods) sampled with a kernel density estimate ($N =$
1317 1000).

1318

1319 **Extended Data Table 3. Sensitivity tests.** Tests of the sensitivity of the ice sheet projections to changes in
1320 the chosen inputs. The test index, name, description and impact are detailed. Numerical values refer to
1321 changes in the median and [5th, 95th] percentile estimates for the ice sheet under SSP5-85, unless otherwise
1322 stated; results for this scenario are shown in Extended Data Figure 4.

1323

1324 **Extended Data Figure 4. Sensitivity of ice sheet projections at 2100 under SSP5-85 to uncertain**

1325 **inputs.** a, Greenland. b, West Antarctica. c, East Antarctica. d, Antarctic Peninsula. Indices refer to test
1326 (see Extended Data Table 3). Box and whiskers show [5, 25, 50, 75, 95]th percentiles. 1: Default; 2:
1327 CMIP6 global climate model ensemble projections of global mean surface air temperature, instead of FaIR
1328 simple climate model; 3: fixed global mean surface air temperature; 4: fixed glacier retreat (Greenland) or

1329 basal melt (Antarctica) parameter. Antarctic regions only: basal melt parameter has 5: 'Mean Antarctic'
1330 distribution; 6: 'Pine Island Glacier' distribution; 7: uniform, high distribution; 8: uniform, very high
1331 distribution. Ice shelf collapse scenario: 9: off and 10: on. 11: Risk-averse projections using the high 'Pine
1332 Island Glacier' distribution for basal melt (test 6), ice shelf collapse on (test 10), and the ice sheet and
1333 climate models that give the highest sea level contributions (Extended Data Figure 5: test 6, 7).

1334

1335 **Extended Data Table 4. Robustness checks.** Checks performed to test the robustness of the ice sheet
1336 projections to changes in the simulation dataset. The test index, name, description and impact are detailed.
1337 Numerical values refer to changes in the median and [5th, 95th] percentile estimates for the ice sheet under
1338 the NDCs scenario, unless otherwise stated; results for this scenario are shown in Extended Data Figure 5.

1339

1340

1341 **Extended Data Figure 5. Robustness of ice sheet projections under Nationally Determined**
1342 **Contributions to ice sheet/climate model simulation selection and treatment.** a, Greenland. b,
1343 West Antarctica. c, East Antarctica. d, Antarctic Peninsula. Indices refer to test (see Extended Data
1344 Table 4). Box and whiskers show [5, 25, 50, 75, 95]th percentiles. 1: Default; 2: Higher resolution ice
1345 sheet models; 3: Ice sheet models with the most complete sampling of uncertainties (10 models for
1346 Greenland, 4 for Antarctica); 4: Single ice sheet model with the most complete sampling of
1347 uncertainties and (coincidentally) high sensitivity to retreat or basal melting parameter. Antarctic
1348 regions only; 5: Alternative single ice sheet model with nearly as complete sampling but low
1349 sensitivity to basal melt parameter. 6: Ice sheet models with the highest sensitivity to basal melt
1350 parameter; 7: Climate models that lead to highest sea level contributions. 8: Ice sheet models with
1351 2015-2020 mass change in the range 0-0.6 cm. 9: Only ice sheet models that use the standard ISMIP
1352 melt parameterisations. 10: Higher basal melt value assigned to ice sheet models that do not use the
1353 standard ISMIP6 melt parameterisations.

1354

1355 **Extended Data Figure 6. Sensitivity to basal melting by Antarctic ice sheet and climate model.**
1356 Vertical lines show ice sheet models that do not use the ISMIP6 basal melt parameterisation, and the
1357 basal melt value they are assigned. Ice sheet models includes the high and low sensitivity models in
1358 Extended Data Figure 5: test 4 (ILTS_PIK/SICOPOLIS) and test 5 (LSCE/GRISLI).

1359

1360 **Extended Data Figure 7. Effect of Antarctic ice shelf collapse by climate model.** Additional sea
1361 level contribution at 2100 when using ice shelf collapse for six climate models, ordered by maximum
1362 impact on the Peninsula contribution. (a) West and (b) East Antarctica, and (c) Peninsula.

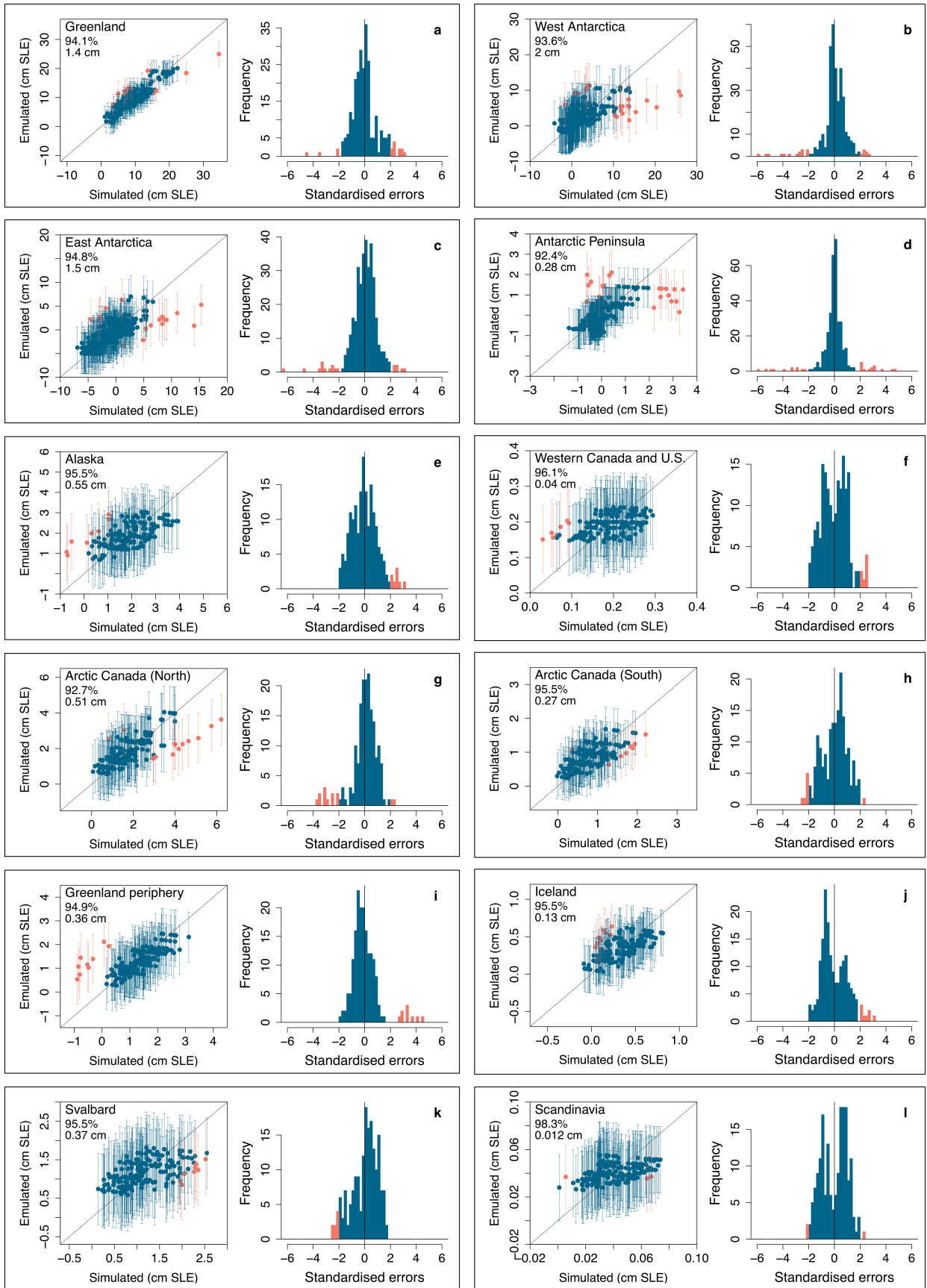
1363

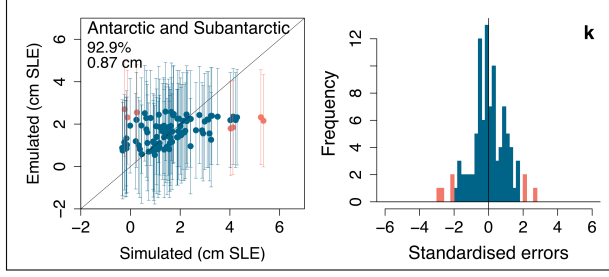
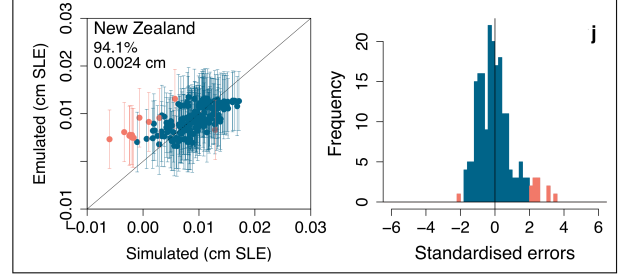
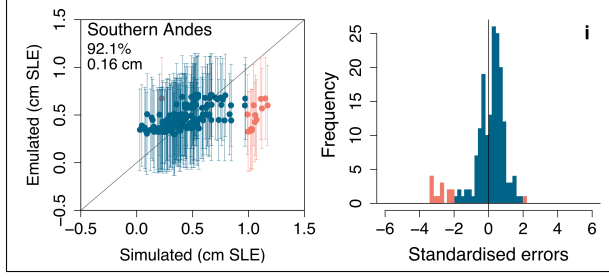
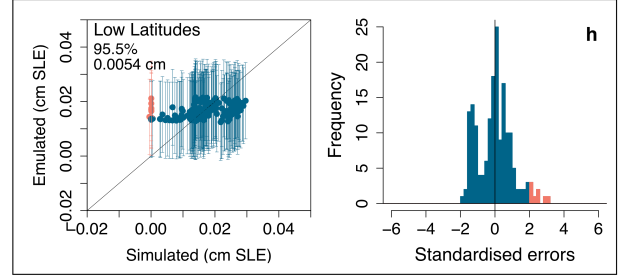
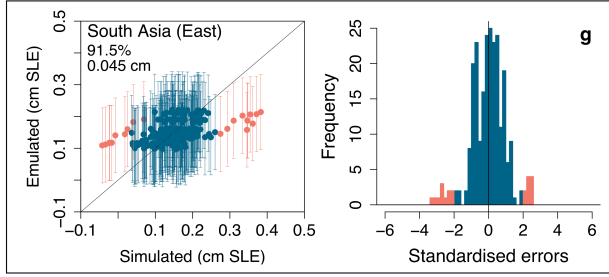
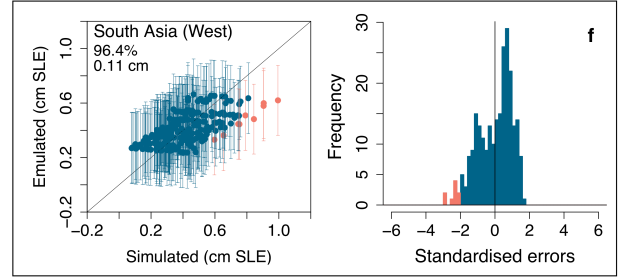
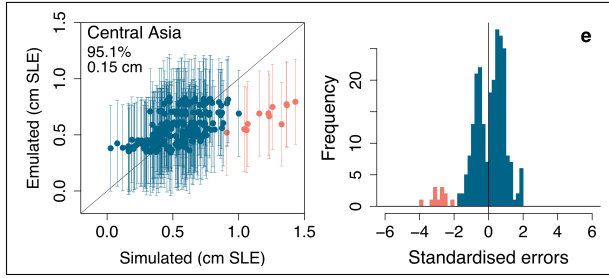
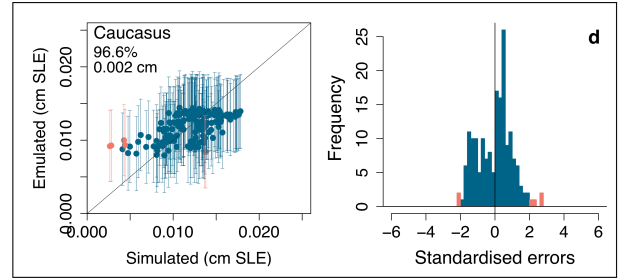
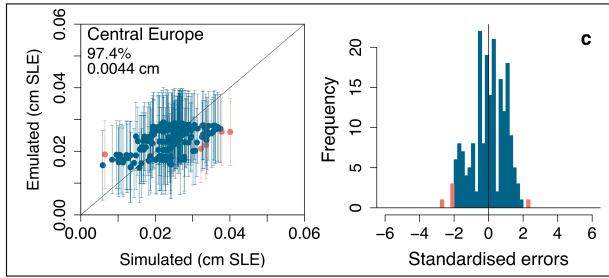
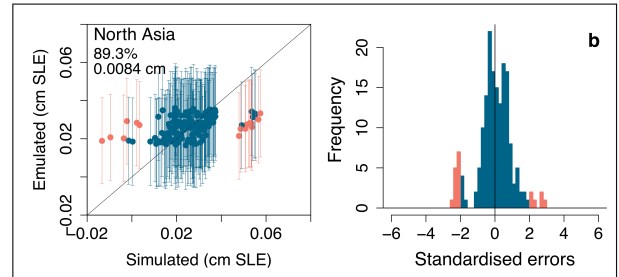
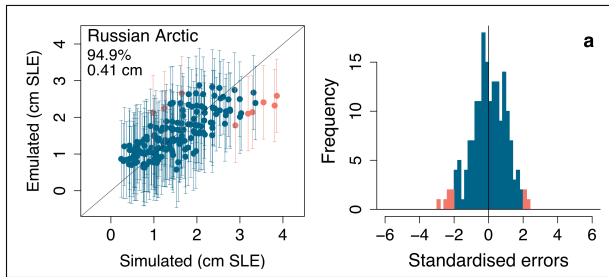
1364

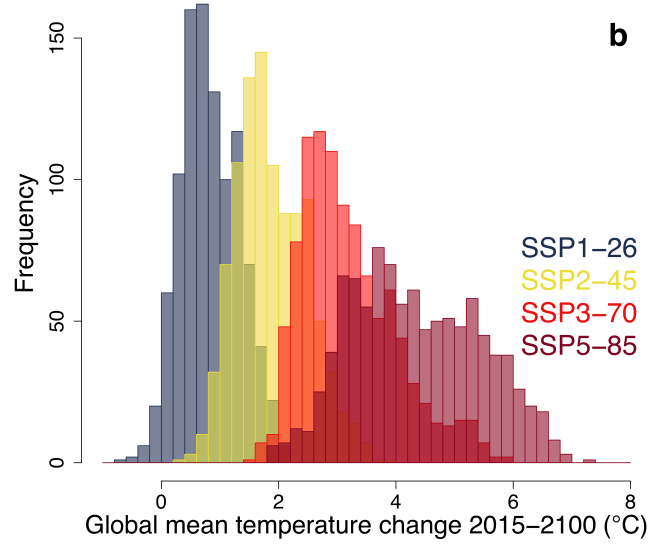
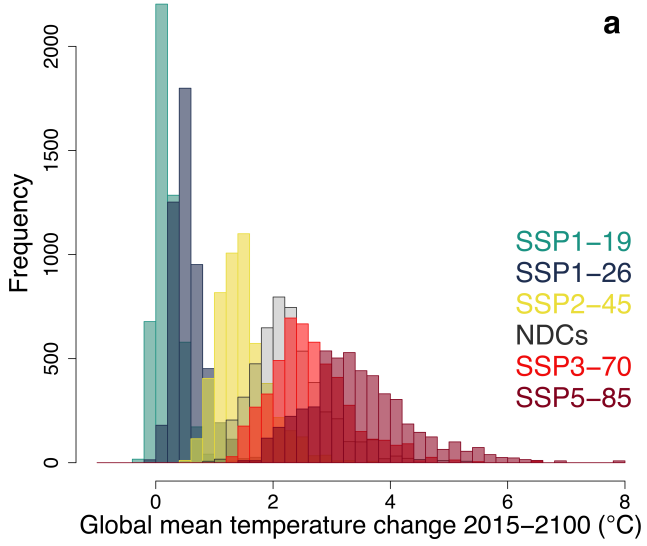
1365

Additional Greenland experiments				
Experiment name	Scenario	Climate model	Retreat parameter	
expe01	RCP8.5	NorESM1-M	K ₉₅	
expe02	RCP8.5	NorESM1-M	K ₅	
expe03	RCP8.5	HadGEM2-ES	K ₉₅	
expe04	RCP8.5	HadGEM2-ES	K ₅	
expe05	RCP2.6	MIROC5	K ₉₅	
expe06	RCP2.6	MIROC5	K ₅	
expe07	RCP8.5	IPSL-CM5A-MR	K ₉₅	
expe08	RCP8.5	IPSL-CM5A-MR	K ₅	
expe09	RCP8.5	CSIRO-Mk3-6-0	K ₉₅	
expe10	RCP8.5	CSIRO-Mk3-6-0	K ₅	
expe11	RCP8.5	ACCESS1-3	K ₉₅	
expe12	RCP8.5	ACCESS1-3	K ₅	
expe13	SSP5-85	CNRM-CM6-1	K ₉₅	
expe14	SSP5-85	CNRM-CM6-1	K ₅	
expe15	SSP1-26	CNRM-CM6-1	K ₉₅	
expe16	SSP1-26	CNRM-CM6-1	K ₅	
expe17	SSP5-85	UKESM1-0-LL	K ₉₅	
expe18	SSP5-85	UKESM1-0-LL	K ₅	
expe21	SSP5-85	CNRM-ESM2-1	K ₉₅	
expe22	SSP5-85	CNRM-ESM2-1	K ₅	
expe23	RCP8.5	MIROC5	K ₉₅	
expe24	RCP8.5	MIROC5	K ₅	
Additional Antarctic experiments				
Experiment name	Scenario	Climate model	Basal melt (γ ₀)	Ice shelf collapse (C)
Basal melt parameter values				
expD1	RCP8.5	MIROC-ESM-CHEM	MeanAnt ₉₅	Off
expD2	RCP8.5	MIROC-ESM-CHEM	MeanAnt ₅	Off
expD3	RCP2.6	NorESM1-M	MeanAnt ₉₅	Off
expD4	RCP2.6	NorESM1-M	MeanAnt ₅	Off
expD5	RCP8.5	CCSM4	MeanAnt ₉₅	Off
expD6	RCP8.5	CCSM4	MeanAnt ₅	Off
expD7	RCP8.5	HadGEM2-ES	MeanAnt ₉₅	Off
expD8	RCP8.5	HadGEM2-ES	MeanAnt ₅	Off
expD9	RCP8.5	CSIRO-Mk3-6-0	MeanAnt ₉₅	Off
expD10	RCP8.5	CSIRO-Mk3-6-0	MeanAnt ₅	Off
expD11	RCP8.5	IPSL-CM5A-MR	MeanAnt ₉₅	Off
expD12	RCP8.5	IPSL-CM5A-MR	MeanAnt ₅	Off
expD13	SSP5-85	CNRM-CM6-1	MeanAnt ₉₅	Off
expD14	SSP5-85	CNRM-CM6-1	MeanAnt ₅	Off
expD15	SSP5-85	UKESM1-0-LL	MeanAnt ₉₅	Off
expD16	SSP5-85	UKESM1-0-LL	MeanAnt ₅	Off
expD17	SSP5-85	CESM2	MeanAnt ₉₅	Off
expD18	SSP5-85	CESM2	MeanAnt ₅	Off
expD51	RCP8.5	NorESM1-M	PIG ₅	Off
expD52	RCP8.5	NorESM1-M	PIG ₉₅	Off
expD53	RCP8.5	MIROC-ESM-CHEM	PIG ₅₀	Off
expD54	RCP8.5	MIROC-ESM-CHEM	PIG ₅	Off
expD55	RCP8.5	MIROC-ESM-CHEM	PIG ₉₅	Off
expD56	RCP8.5	CCSM4	PIG ₅₀	Off
expD57	RCP8.5	CCSM4	PIG ₅	Off
expD58	RCP8.5	CCSM4	PIG ₉₅	Off
expT071	RCP2.6	NorESM1-M	PIG ₅₀	Off
expT072	RCP2.6	NorESM1-M	PIG ₅	Off
expT073	RCP2.6	NorESM1-M	PIG ₉₅	Off
Ice shelf collapse under different climate forcings				
expE6	RCP8.5	NorESM1-M	MeanAnt ₅₀	On
expE7	RCP8.5	MIROC-ESM-CHEM	MeanAnt ₅₀	On
expE8	RCP8.5	HadGEM2-ES	MeanAnt ₅₀	On
expE9	RCP8.5	CSIRO-Mk3-6-0	MeanAnt ₅₀	On
expE10	RCP8.5	IPSL-CM5A-MR	MeanAnt ₅₀	On
Ice shelf collapse and basal melt interactions				
expTD5	RCP8.5	CCSM4	MeanAnt ₉₅	On
expTD56	RCP8.5	CCSM4	PIG ₅₀	On
expTD58	RCP8.5	CCSM4	PIG ₉₅	On

Region	Covariance function and hyperparameters (α : exponent; ν : roughness parameter)	% predictions within emulator 95% interval	Mean absolute error (cm)
Greenland ice sheet	power exp ($\alpha = 0.1$)	94.1	1.4
West Antarctica	power exp ($\alpha = 0.1$)	93.6	2.0
East Antarctica	power exp ($\alpha = 0.1$)	94.8	1.5
Antarctic Peninsula	power exp ($\alpha = 0.1$)	92.4	0.28
1: Alaska	power exp ($\alpha = 1.0$)	95.5	0.55
2: Western Canada and U.S.	power exp ($\alpha = 1.9$)	96.1	0.040
3: Arctic Canada North	power exp ($\alpha = 1.9$)	92.7	0.51
4: Arctic Canada South	power exp ($\alpha = 0.1$)	95.5	0.27
5: Greenland periphery	power exp ($\alpha = 0.1$)	94.9	0.36
6: Iceland	power exp ($\alpha = 1.0$)	95.5	0.13
7: Svalbard	power exp ($\alpha = 0.1$)	95.5	0.37
8: Scandinavia	power exp ($\alpha = 1.0$)	98.3	0.012
9: Russian Arctic	power exp ($\alpha = 1.0$)	94.9	0.41
10: North Asia	power exp ($\alpha = 1.0$)	89.3	0.0084
11: Central Europe	power exp ($\alpha = 1.0$)	97.4	0.0044
12: Caucasus	Matérn ($\nu = 3/2$)	96.6	0.0020
13: Central Asia	power exp ($\alpha = 0.1$)	95.1	0.15
14: South Asia (West)	power exp ($\alpha = 1.9$)	96.4	0.11
15: South Asia (East)	power exp ($\alpha = 0.1$)	91.5	0.045
16: Low Latitudes	power exp ($\alpha = 0.1$)	95.5	0.0054
17: Southern Andes	Matérn ($\nu = 5/2$)	92.1	0.16
18: New Zealand	power exp ($\alpha = 0.1$)	94.1	0.0024
19: Antarctic and Subantarctic periphery	Matérn ($\nu = 5/2$)	92.9	0.87

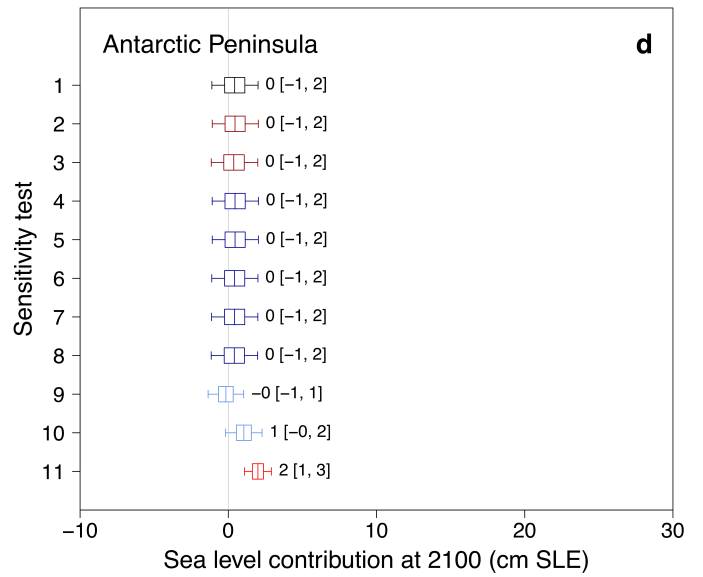
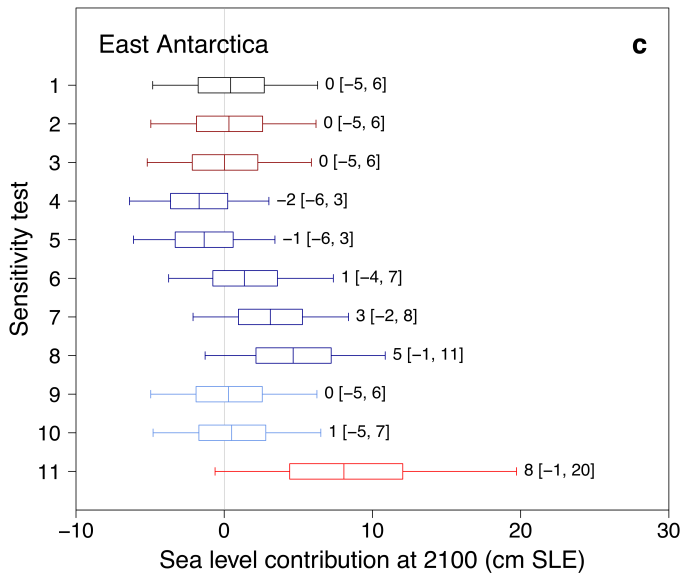
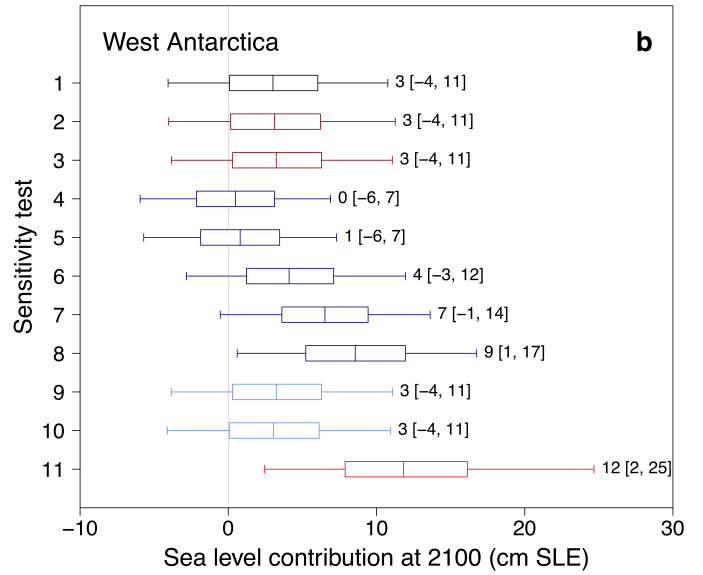
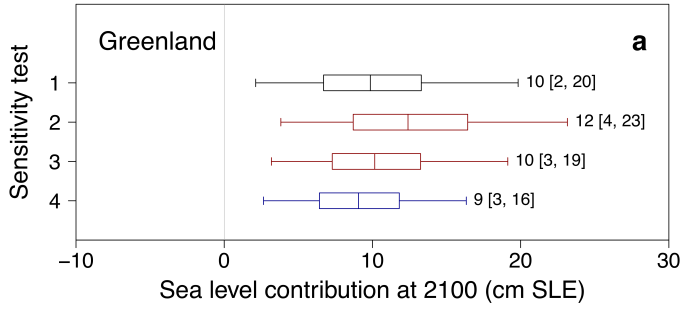






Sensitivity tests

Description	Impact
2: CMIP6 temperature projections	
<p>Around 30 CMIP6 models are available at the time of analysis for four SSPs (31 for SSP1-26, 30 for SSP2-45, 27 for SSP3-70 and 31 for SSP5-85). Simulations are obtained and processed in the same way as the subset used for the emulator calibration. We set missing 2100 values to that of 2099 (for CAMS-CSM1-0, and two additional models for SSP3-70). We smooth the temperature changes with a kernel density estimator and sample from this with replacement (N = 1000; Extended Data Figure 3).</p>	<p>We find a slight increase in projected sea level rise: median and 95th percentile land ice contributions increase by 1-5 cm and 4-7 cm across scenarios SSP1-26 to SSP5-85. This is likely due to the greater number of simulations with high equilibrium climate sensitivity in CMIP6 than FaIR (and a wider range than several recent past generations, 1.8-5.6°C)³⁴. The FaIR ensemble is constructed to have a climate sensitivity distribution in line with latest understanding from multiple lines of evidence (5-95% range 2-5°C)³⁰.</p>
3, 4: Fixed global mean temperature and ice sheet melt parameters	
<p>We replace the input distributions with single values, to test the potential for reducing uncertainties with improved knowledge</p>	<p>Using the FaIR ensemble mean for global temperature, the width of the 5-95% range for SSP5-85 reduces from 30 cm to 26 cm. Using default values of the Greenland retreat and Antarctic basal melt parameters ($\kappa = \kappa_{50}$; $\gamma_0 = \text{MeanAnt}_{50}$), the 5-95% range decreases from 30 cm to 25 cm.</p>
5, 6: Antarctic basal melt - Mean Antarctic and Pine Island Glacier distributions	
<p>We use the Mean Antarctic (test 5), or Pine Island Glacier (test 6) distribution for basal melt γ, rather than the combined distribution, sampling from the original distributions with replacement.</p>	<p>Results are discussed in the main text.</p>
7, 8: Antarctic basal melt - uniform distributions	
<p>We use two uniform distributions to reproduce the sampling strategy of ref [26]. This is an emulation-type study based on a similar ensemble of climate and Antarctic ice sheet models to ISMIP6, which uses a uniform distribution for basal melt sensitivity consistent with values estimated for the Amundsen Sea region³⁹. If we add projections of dynamic change from ref. [26] to IPCC AR5²⁵ projections for surface mass balance (SMB), neglecting differences in time period, the median projections are ~11 and ~13 cm under RCP2.6 and RCP8.5, and the 95th percentiles are ~35 and ~54 cm (using median SMB values in both).</p>	<p>We reach similar values only with extreme values of the basal melt parameter: we show here $\gamma \sim \text{unif}[\text{PIG}_{50}, \text{PIG}_{95}]$ and $\gamma \sim \text{unif}[\text{PIG}_{50}, 700000]$, where 700000 is 98.7th percentile of the Pine Island Glacier distribution, which give median projections of 10 cm and ~14 cm across all scenarios. The 95th percentiles are roughly half those of the other study: ~19 cm and ~24 cm.</p>
9, 10: Antarctic ice shelf collapse off and on	
<p>We use only $C = 0$ or $C = 1$, rather than a random sample of the two.</p>	<p>Results are discussed in the main text.</p>
11: Risk-averse Antarctic projections	
<p>We use the five global climate models with highest sea level contribution or for which ice shelf collapse projections are available (Robustness test 7), the four Antarctic ice sheet models with highest sensitivity to basal melting (Robustness test 6), the Pine Island Glacier distribution for basal melt γ (Sensitivity test 6) and ice shelf collapse on (Sensitivity test 10). We also use the same γ value for all three regions in a given projection, i.e. fully correlated rather than sampled independently, to explore the tails more fully: this aspect broadens the distribution, increasing the 95th percentile by 2-4 cm and decreasing the 5th by 1 cm, and also decreases the median by 1 cm. We use N = 5000 temperature samples, as for the main projections. We do not use the combinations that lead to the highest possible sea level contribution – i.e. the single most sensitive ice sheet model (Robustness test 4), or the extreme distributions for basal melt (Sensitivity test 7-8) – because we aim to provide plausible high-end projections, rather than relying on a single model or unrealistic assumptions.</p>	<p>Results are discussed in the main text.</p>



Robustness checks	
Description	Impact
2: High resolution models	
We use only Greenland ice sheet models with minimum spatial resolution less than 8 km (N = 215) and Antarctic ice sheet models with resolution less than 32 km (N = 303).	This results in differences of 0-1 cm for each ice sheet.
3: More balanced design	
We restrict the input dataset to only the models with the most complete designs (i.e. the most experiments). For Greenland, we use 10 of the 21 models: one with 28 experiments (IMAU/IMAUICE1) and the nine models that ran all 14 experiments presented by refs. [14] and [16] (AWI/ISSM1, ISSM2 and ISSM3, ILTS_PIK/SICOPOLIS1 and SICOPOLIS2, JPL/ISSM, LSCE/GRISLI2, NCAR/CISM, VUB/GISMHOMv1), removing the dummy variable from the emulator as there are no 'open' models in this set (N = 154). For Antarctica, we use four of the 16 models (ILTS_PIK/SICOPOLIS: N = 55, of which 13 do not use the ISMIP6 parameterisation; JPL1/ISSM: N = 48; LSCE/GRISLI: N = 47; NCAR/CISM: N = 27) (total N = 177).	This results in differences of 0-1 cm for each ice sheet.
4, 5: Single ice sheet models	
We use only the Greenland model with the most simulations (IMAU/IMAUICE1: N = 28), and a single model for Antarctica (test 4: ILTS_PIK/SICOPOLIS, N = 48; test 5: LSCE/GRISLI, N = 47). The two Antarctic models have high and low sensitivity to the basal melting parameter, respectively (Extended Data Figure 6).	Using one Greenland model has little impact: the largest change is 2 cm increase in the 95 th percentile, due to this model being at the upper end of the range in sensitivity to the retreat parameter (Figure 2a: triangles). Using one Antarctic model has far more effect: results are discussed further in the main text.
6: Highest sensitivity Antarctic ice sheet models	
We use the four Antarctic models with highest sensitivity to basal melting, i.e. largest 2100 contribution for $\gamma = \text{PIG}_{50}$, ice shelf collapse off and RCP8.5/SSP5-85 (decreasing order: ILTS_PIK/SICOPOLIS: N = 48; ULB/fETISH_16km: N = 21; ULB/fETISH_32km: N = 21; DOE/MALI: N = 8) (total N = 98).	Results are discussed in the main text.
7: Select climate models that result in highest Antarctic sea level contributions	
We use only results from the climate models that lead to highest sea level contributions at 2100 under $\gamma = \text{MeanAnt}_{50}$, ice shelf collapse off and RCP8.5/SSP5-85 (in decreasing order: HadGEM2-ES, UKESM1-0-LL, MIROC-ESM-CHEM, NorESM1-M). We also include CCSM4, to retain information on the effect of ice shelf collapse (N = 241). We also test the impact of using only two of these climate models (not shown in Extended Data Figure 5): NorESM1-M (discussed in the main text regarding scenario-dependence: Figure 4) and CCSM4 (for shelf collapse) (N = 164).	Using these five climate models results in +1 cm change to median from SSP1-19 to SSP5-85 for West Antarctica, -1 cm for East Antarctica, and +1 cm for the total. NDCs median increases by +2 cm relative to main projections. Using only NorESM1-M and CCSM4 leads to +2 cm from SSP1-19 to SSP5-85 for West Antarctica, -3 cm for East Antarctica, and -3 cm decrease for the total, i.e. a weak scenario dependence; no change to NDCs median.
8: Exclude Antarctic ice sheet models far from observed trend	
We exclude simulations with 2015-2020 sea level contributions outside the range 0.00-0.60 cm, motivated by recent observations. We use a satellite estimate ⁶⁶ of the mass trend from 2012-2017 ($-219 \pm 43 \text{ Gt a}^{-1}$) and reject simulations for which the mean trend over 2015-2020 is outside the mean ± 5 s.d. interval (N = 181). We choose this interval to allow for the trend changing from one time period to the other, and for tolerance to model discrepancy ²⁴ , and because it coincides with zero at the bottom end so is informative for excluding models with mass gain at the start of the projections (as well as those with very rapid mass loss).	This results in +1 cm scenario-dependence for West Antarctica and -2 cm for East Antarctica, and none for the total; the NDCs median increases by 1 cm.
9: Exclude Antarctic ice sheet models that do not use ISMIP6 melt parameterisation	
We exclude the ice sheet models that do not use the ISMIP6 basal melt parameterisation. (N = 282).	No scenario-dependence for West Antarctica or the total; -2 cm for East Antarctica. No change to NDCs median.
10: Impute higher basal melt value for Antarctic ice sheet models that do not use the ISMIP6 melt parameterisation	
We assign models that do not use the ISMIP6 parameterisations a higher value for γ (150,000; slightly less than PIG_{50}), rather than the ensemble mean (59,317), reflecting the fact that such models are often tuned to Amundsen Sea (high) melt observations, and approximately in line with NCAR/CISM which was run in both modes (Extended Data Figure 6).	This results in +1 cm scenario-dependence for West Antarctica, -1 cm decrease for East Antarctica, and no change for the total; the NDCs median projection decreases by 1 cm.

